



Peter Tumfart, BSc

Decoding of range during goal-directed movement preparation using EEG

MASTER'S THESIS

to achieve the university degree of

Diplom-Ingenieur

Master's degree programme: Biomedical Engineering

submitted to

Graz University of Technology

Supervisor

Univ.-Prof. Dipl.-Ing. Dr.techn. Gernot R. Müller-Putz

Institute of Neural Engineering

Graz, September 2023

Abstract

Many brain regions are involved in the processing of goal-directed voluntary movements. While current brain-computer interfaces (BCIs) use brain signals around movement execution as their control signals, activation during movement preparation has little application and little research has been conducted on whether parameters can be extracted that can contribute relevant information to the planned movement. In this work, the possibility of extracting a range parameter from the electroencephalogram (EEG) during the movement preparation phase was investigated. For this purpose, a paradigm was developed in which different distances from different movement directions could be executed and distinguished. In this context, the EEG was measured and analyzed in the delta band, first during movement preparation (aligned with the signaling of a movement target) and secondly during movement execution. In addition, shrinkage Linear Discriminant Analysis (sLDA) classifiers were trained to discriminate between different ranges, motion directions, and positions, and a general linear model (GLM) was used to identify electrodes that mainly contribute to range or direction. During movement preparation, modulations of amplitudes were found mainly at frontal and central electrodes, with significant differences between near and far movements at the studied electrodes. Classification between near and far movements achieved a maximum accuracy of 64% and was significantly above chance level for a period of 0.5 s after a target cue and independent of the movement direction. The evaluation of the GLM showed that especially frontal electrodes encode information about the range of a movement.

Keywords: Electroencephalogram (EEG), Goal-directed movement, Event-related potential (ERP), Movement-related cortical potential (MRCP), Brain-computer interface (BCI).

Kurzfassung

An der Verarbeitung zielgerichteter und freiwilliger Bewegungen sind viele Hirnregionen beteiligt. Während aktuelle Hirn-Computer-Schnittstellen (BCIs) Hirnsignale rund um die Bewegungsausführung als Steuersignale nutzen, finden Hirnsignale während der Bewegungsvorbereitung kaum Anwendung. Weiters wurde wenig darüber geforscht, ob in der Phase der Bewegungsplanung Parameter aus dem EEG extrahiert werden können, die relevante Informationen zur geplanten Bewegung beitragen können. In dieser Arbeit wurde untersucht, ob es möglich ist, bereits in der Phase der Bewegungsvorbereitung einen Distanzparameter aus dem Elektroenzephalogramm (EEG) zu extrahieren. Zu diesem Zweck wurde ein Paradigma entwickelt, in dem verschiedene Distanzen aus unterschiedlichen Bewegungsrichtungen ausgeführt und unterschieden werden können. Dabei wurde das EEG gemessen und im Deltaband, zum einen während der Bewegungsvorbereitung (ausgerichtet an der Signalisierung eines Bewegungsziels) und zum anderen während der Bewegungsausführung, analysiert. Darüber hinaus wurden shrinkage Linear Discriminant Analysis (sLDA) Klassifikatoren trainiert, um zwischen verschiedenen Entfernung, Bewegungsrichtungen und Positionen zu unterscheiden, und ein generelles lineares Modell (GLM) wurde verwendet, um jene Elektroden zu ermitteln, die hauptsächlich zur Entfernung oder Richtung beitragen. Während der Bewegungsvorbereitung konnten vor allem an frontalen und zentralen Regionen Modulationen der Amplituden gefunden werden mit signifikanten Unterschieden zwischen weiten und kurzen Bewegungen an untersuchten Elektroden. Die Klassifizierung zwischen kurzen und weiten Bewegungen erzielte eine maximale Genauigkeit von 64% und lag für einen Zeitraum von 0,5 s signifikant über dem Zufallsniveau, unabhängig von der Bewegungsrichtung. Die Auswertung des GLM zeigte, dass besonders frontale Elektroden Informationen über die Distanz einer Bewegung beinhalteten.

Keywords: Elektroenzephalogram (EEG), Zielgerichtete Bewegung, Ereigniskorreliertes Potential (ERP), Bewegungskorreliertes kortikales Potenzial (MRCP), Gehirn-Computer Schnittstelle (BCI).

Acknowledgements

I would like to express my gratitude to my family, my partner and my friends for their support, encouragement, and understanding throughout my studies and this thesis.

I am also immensely thankful to my supervisor, Prof. Gernot Müller-Putz for his guidance, expertise and mentorship throughout this thesis. Further, I would like to thank Dr. Valeria Mondini her valuable inputs during the planning of the paradigm and for her support during the measurements. Also I would like to express my gratitude to all the members of the Institute of Neural Engineering for their support and kind reception.

Finally, I would like to thank all participants for their participation and cooperation in this study .

Contents

1	Introduction	1
1.1	Motivation and aim	4
2	Methods	5
2.1	Experimental Design	5
2.1.1	Participants	5
2.1.2	Data recording	5
2.1.3	Setup	6
2.1.4	Procedure	8
2.2	Pre-processing	11
2.3	Temporal analysis	15
2.3.1	Statistical analysis	15
2.4	Classification analysis	16
2.4.1	Linear discriminant analysis (LDA)	16
2.4.2	Application of sLDA	18
2.5	Encoding of distance and direction/position	21
2.5.1	General linear model (GLM)	21
3	Results	25
3.1	Temporal results	25
3.1.1	Movement timings	25
3.1.2	Grand average results	26

3.2	Classification results	30
3.2.1	Range classifier	30
3.2.2	Direction classifier	33
3.2.3	Position classifier	42
3.3	Encoding of range and direction	47
3.3.1	Cue-aligned	47
3.3.2	Movement-aligned	49
4	Discussion	53
4.1	Temporal results	53
4.2	Classification analysis	54
4.3	Encoding of range and direction	56
5	Conclusion	58
	Bibliography	60

List of Figures

1.1	Procedure of movement planning to execution	2
2.1	Positions of the EEG electrodes	6
2.2	Experimental setup	7
2.3	Timing of the execution paradigm	9
2.4	Types of trials.	10
2.5	Timing of the eye paradigm.	12
2.6	Pre-processing pipeline.	13
2.7	Leave-one-out cross-validation scheme.	20
3.1	Box plots of the movement timings.	26
3.2	Grand average results for cue-aligned epoching.	28
3.3	Grand average results for movement-aligned epoching.	31
3.4	Range classification cue-aligned.	32
3.5	Range classification movement-aligned.	34
3.6	Direction classification cue-aligned.	36
3.7	Near direction classification cue-aligned.	37
3.8	Far direction classification cue-aligned.	39
3.9	Direction classification movement-aligned.	40
3.10	Near direction classification movement-aligned.	42
3.11	Far direction classification movement-aligned.	43
3.12	Position classification cue-aligned.	45
3.13	Position classification movement-aligned.	46

3.14	GLM results cue-aligned for the regression coefficients.	48
3.15	GLM results cue-aligned comparing the conditions.	49
3.16	GLM results movement-aligned for the regression coefficients.	51
3.17	GLM results movement-aligned comparing the conditions.	52

List of Acronyms and Symbols

BCI	Brain-computer interface
BP	Bereitschaftspotential
BTT-f	Bottom-to-top far
BTT-n	Bottom-to-top near
CAR	Common Average Reference
CV	Cross-validation
EEG	Electroencephalogram
EOG	Electrooculogram
GLM	General linear model
LED	Light-emitting diode
LDR	Light dependent resistor
LOO	Leave-one-out
LSL	Lab streaming layer
LTR-f	Left-to-right far
LTR-n	Left-to-right near
MRCP	Movement-related cortical potential
OLS	Ordinary least squares
RLS	Regularized least squares
RTL-f	Right-to-left far
RTL-n	Right-to-left near
SCI	Spinal cord injury
SD	Standard deviation
SGEYESUB	Sparse generalized eye artifact subspace subtraction
sLDA	Shrinkage linear discriminant analysis
SMA	Supplementary motor area
TTB-f	Top-to-bottom far
TBB-n	Top-to-bottom near

1 Introduction

Reaching for a glass of water, grabbing a car key, or reaching for a pen — actions that are performed countless times every day, automated and without much thought. However, this is only true if you have control over your upper limbs. What if this is not the case, for example, after tetraplegia? In such cases, assistive technologies can be used to restore or replace function. One approach is to use a brain-computer interface (BCI), a system that measures brain activity and converts it into control commands to operate a neuroprosthesis or a robotic arm, for example [1].

To develop and improve such BCIs, it is important to understand how movements, which seem simple at first sight, are represented in the human brain. The processing that takes place in planning voluntary movements involves many brain regions (Fig. 1.1). First, visual input is received by the primary visual cortex and then processed by the ventral and dorsal streams [2]. The ventral stream, also known as the “where” stream, is related to object processing with features such as color, texture, or size of an object and moves along the ventral surface to the medial temporal lobe [3]. The dorsal stream, also known as the “what” stream, is associated with spatial processing such as location, movement, and spatial relations and delivers information via the dorsal surface to the posterior parietal cortex [3]. Afterwards, this data is transmitted to the prefrontal cortex and premotor areas. In the prefrontal cortex, the decision-making and organization of a movement take place in terms of timing and type of movement [4]. The premotor cortex, while having some neuronal connections to motor neurons, is the main region for movement planning and preparation of a movement [5]. Finally, when

all the planning is done, the primary motor cortex controls the correct motor neurons for the movement execution [6].

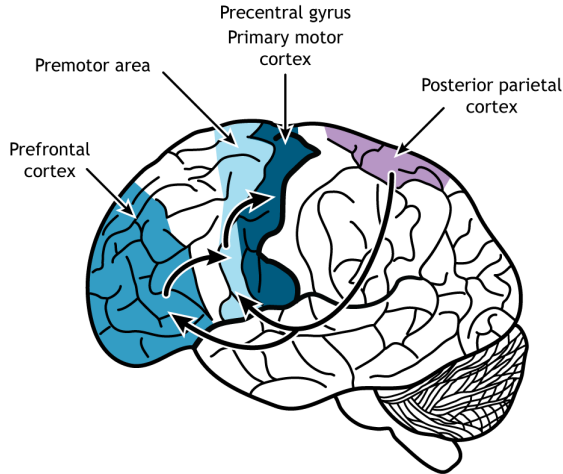


Figure 1.1: Procedure of movement planning to execution with the involved areas on the cortex [7].

Modern non-invasive BCIs mainly use electroencephalography (EEG) to measure electrical activity originating from the brain [8]. EEG is generated mainly by the summed excitatory postsynaptic potentials of many apical dendrites that are aligned at the outer layer of the cortex, covering an area of approximately 1 to 6 cm^2 [9]. The EEG can be measured using metal electrodes, which are usually made of silver/silver chloride. For this purpose, the electrodes are placed on the scalp and contacted with conductive gel. A biosignal amplifier amplifies and filters the signal to make the signals analyzable [10].

While earlier BCIs used motor imagery as their main strategy, which utilize well distinguishable sensorimotor rhythms generated by different imaginations [11], currently developed BCIs use a more intuitive approach to extract control commands [12]. Intuitive in that sense means, that the user should behave as if they would actually perform the desired action and the BCI directly extracts the desired control commands [12]. Therefore, the brain signals that are used by the BCI are in direct relation to the movement, so-called movement-related cortical potentials (MRCPs). MRCPs can be

measured using EEG in central brain regions with frequencies in the delta band of 1 to 4 Hz and originate from the supplementary motor area (SMA) and the motor cortex [13]. They are subdivided into pre-movement and post-movement components. The pre-movement component consists of the Bereitschaftspotential (BP), a slowly rising negativity, starting as early as 1.5 s prior to the movement and a late negativity starting around 400 ms before the movement onset, which is a steeper negative potential shift and is highest on the contralateral central electrodes [14], [15]. The post-movement component manifests in a positive shift right after the movement onset [16].

Collinger et al. demonstrated the control of a prosthetic limb in a three-dimensional environment with seven degrees of freedom using implanted intracortical electrodes recording spiking activity in a tetraplegic individual [17]. Research projects like MoreGrasp¹ or FeelYourReach² built non-invasive BCI systems towards controlling upper limb neuroprostheses by decoding EEG patterns associated with voluntary movements [8], [12]. Numerous studies investigated neural correlates in upper limb movements with respect to kinematic parameters like direction, speed, acceleration and type of movement [18]. Ofner et al. were able to discriminate between different forms of upper limb movement [19]. Mondini et al. showed the possibility of continuously decoding trajectories from low frequency EEG in order to control a robotic arm in an online scenario by regressing positions, velocities and accelerations [20]. Pereira et al. developed a paradigm to asynchronously detect self-initiated movement onset from MRCPs, which is an important factor for the applicability of this system for individuals with spinal cord injury (SCI) [21].

While the aforementioned work dealt with neural correlates around the execution of movement, Kobler et al. (2020) were able to show in a center-out paradigm that information about the direction of a voluntary upper limb movement is already encoded in the preparation phase, i.e., phase-locked to a cue instead of phase-locked to the

¹<http://www.moregrasp.eu/>

²<https://www.tugraz.at/institute/ine/research/team-mueller-putz/feel-your-reach/>

movement onset, in the delta band EEG [22].

1.1 Motivation and aim

The aim of this thesis is to investigate the neural processes underlying the encoding of the range towards a discrete target in movement preparation, initiation and execution. More figuratively speaking: How far away is the glass of water? Providing a novel range parameter may prove useful in future BCI systems, for example, as an additional control parameter prior to the movement, increasing the confidence of movement decoders during goal-directed movements.

Following the work of Kobler et al. (2020), we conclude that it should be possible to extract a range parameter from the low-frequency EEG already in the phase of movement preparation (aligned to a target cue). Therefore, the following hypotheses have been stated:

It is possible to decode the range towards a discrete target in a reaching task from delta band EEG during movement preparation and execution.

A possible range parameter is independent of the direction of motion.

To test these hypotheses, a paradigm was developed in which different distances and different directions of the movements could be investigated.

2 Methods

This chapter provides a detailed description of the experimental design, data recording, pre-processing steps and processing analysis employed in this thesis, with the aim of explaining the investigation procedure in an understandable way and providing a guide for repeating the same.

2.1 Experimental Design

2.1.1 Participants

Ten healthy and right-handed subjects (2 females, 8 males) aged 24.6 ± 2.5 (mean \pm standard deviation (SD)) years voluntarily participated in this study. The subjects had normal or corrected-to-normal vision. After detailed verbal and written instruction, all participants gave written informed consent to participate in this study. All participants were seated in a comfortable position, with the experimental board placed approximately 30 cm in front of them. The height of the chair was adjusted so that all targets on the board were within reach of their right arm without having to leave their seated position. The experiment took place in a shielded measurement box to minimize the influence of electromagnetic noise from the environment.

2.1.2 Data recording

EEG activity was recorded using 64 active electrodes with the actiCAP system and two BrainAmp biosignal amplifiers (Brain Products GmbH, Munich, Germany) at a

sampling rate of 256 Hz. Of the 64 electrodes, 61 were used as EEG electrodes and 3 electrodes recorded the electrooculogram (EOG). Figure 2.1 shows the positions of the EEG electrodes on the scalp, which were placed according to the international 10-10 system [23]. The 3 EOG electrodes were placed below the outer corners of the eyes and above the nasion, as described by Lopes-Dias et al. [24]. The ground and reference electrodes were placed at position AFz and at the right mastoid, respectively.

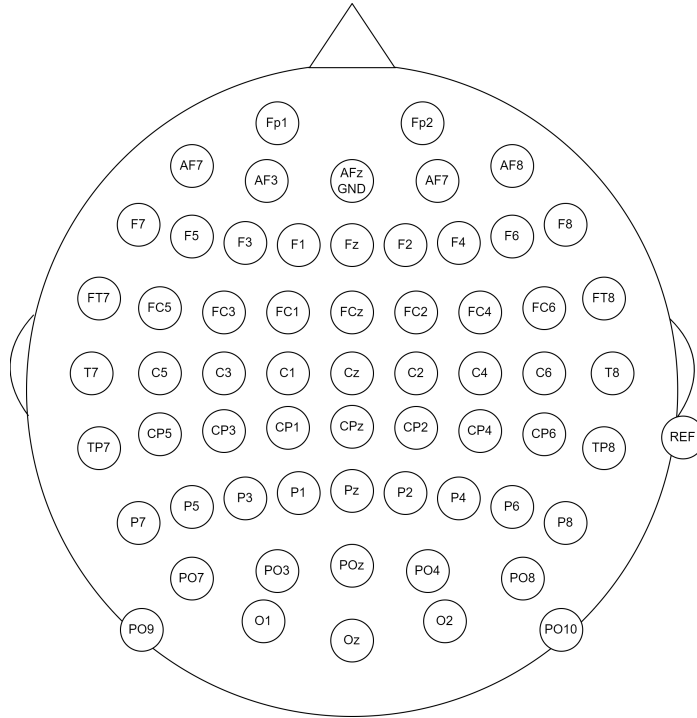


Figure 2.1: Positions of the EEG electrodes with the ground electrode (GND) on position AFz and the reference electrode (REF) at the right mastoid.

2.1.3 Setup

To investigate the previously mentioned hypotheses, a vertical board (width = 70 cm and height = 60 cm) with five discrete targets was built. The board consisted of five handles placed in the shape of a “plus” at evenly spaced intervals on the board. The distance between the anchor points was 20 cm (Figure 2.2 A). A green light-emitting diode (LED) was placed in the center of each handle and a light-dependent resistor (LDR) was placed

on the right side in order to detect touches and releases. Both the LED and the LDR were flush mounted in order not to interfere with the subjects' grasping.

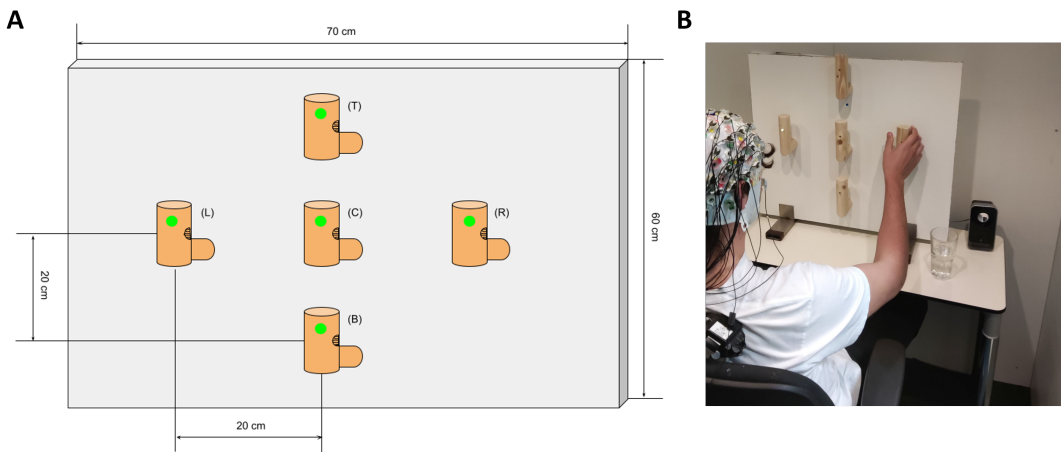


Figure 2.2: **A:** Drawing of the experimental board, showing the placements of the targets, the LEDs and the LDRs. Green dots indicate the LEDs, black half circles with a meander indicate the LDRs. **B:** Setup of the experiment with a participant executing a trial.

The LEDs and the LDRs were wired to an Arduino Uno board that has an AT-Mega328P microcontroller¹. A simple serial command handler was written on the microcontroller to control the LEDs (turning them on and off) and to read the states of the LDRs (light or dark) from the central paradigm script.

Prior to the experiments, the thresholds for each LDR were adjusted to the light settings of the measurement box to obtain a responsive but also robust detection marker for touch and release of the handles.

The experimental paradigm was implemented using MATLAB (The MathWorks Inc., Natick, Massachusetts, USA). This script took care of the timings, the communication with the microcontroller and the streaming of the paradigm markers using the lab streaming layer (LSL)² which syncs the events of the experiment board with the EEG recordings.

¹The written firmware can be found here: <https://github.com/petertumfart/decoding-of-range-EEG>

²<https://github.com/sccn/labstreaminglayer>

2.1.4 Procedure

The experiment was divided into 11 blocks, of which 9 blocks were reaching and grasping blocks, later referred to as execution blocks, and 2 blocks were for recording ocular artifacts and resting-state EEG activity, later referred to as eye blocks. An execution block lasted 7 minutes on average and an eye block lasted 6 minutes on average. The entire experiment lasted 2.5 to 3 hours, including participant briefing, EEG preparation, execution of the experiment, and breaks.

2.1.4.1 Execution block

Paradigm

An execution block consisted of 40 trials with eight different conditions distributed pseudo-randomly. At the start of a trial, a green LED lit up for 2 seconds on one of the outer handles, indicating the starting position. The participants were instructed to move their right arm from the resting position — the arm resting comfortably on the table in front of them — to the indicated starting handle and grasp it in a continuous motion using as few extra muscles as possible. This was followed by a 5-second cue period indicated by the illumination of a green LED on one of the other targets, which was the target handle. Participants were instructed to wait approximately 1 second before reaching for the target handle. This was a crucial part of later being able to distinguish between cue-based and movement-based cortical activation. The handle was held until a beep sounded. This audible signal indicated the end of the cue period and the beginning of the break, which lasted between 3 and 4 seconds. During this break, participants returned their arm to the rest position and were able to perform artifacts such as blinking, swallowing, and adjusting their posture. Figure 2.3 shows the timing of one trial of the execution block; illustrated is one example condition.

Trial types

Figure 2.4 shows the 8 different conditions. Each trial started at one of the outer handles, leading to four supercategories. These 4 supercategories were designated left-

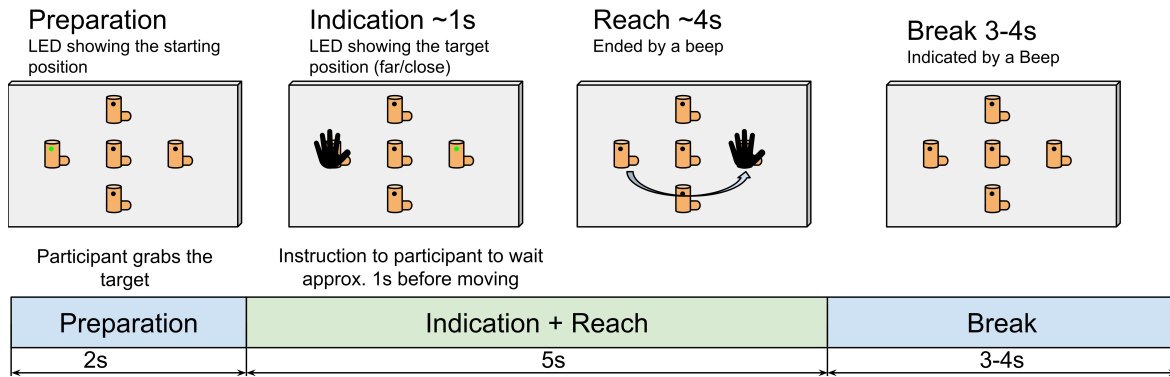


Figure 2.3: Timing of one trial on the example of a far left-to-right condition. Starting with a 2 second preparation period indicating the start position, followed by a 5 seconds cue period indicating the target position and ending with a 3 - 4 second break period.

to-right (LTR), right-to-left (RTL), bottom-to-top (BTT), and top-to-bottom (TTB). From each starting position, only the two target handles were possible, aligned with the center handle and the start handle. This resulted in a near movement when the target was the middle handle and a far movement when the target was the opposite handle. Therefore, a suffix was added to each of the 4 supercategories to indicate whether the movement was near (-n) or far (-f). This resulted in the following 8 conditions: LTR-n, LTR-f, RTL-n, RTL-f, BTT-n, BTT-f, TTB-n, and TTB-f.

A trial was considered correct when all of the following 4 requirements were fulfilled:

- (i) A touch of the starting handle was detected within the 2 s preparation period.
- (ii) The release of the starting handle was detected during the 5 s indication and reach period.
- (iii) The touch of the target handle was detected during the 5 s indication and reach period, but after the release of the starting handle.
- (iv) No other touches/releases were detected before the break period.

Trials that did not fulfill the requirements above were rejected from further analysis.

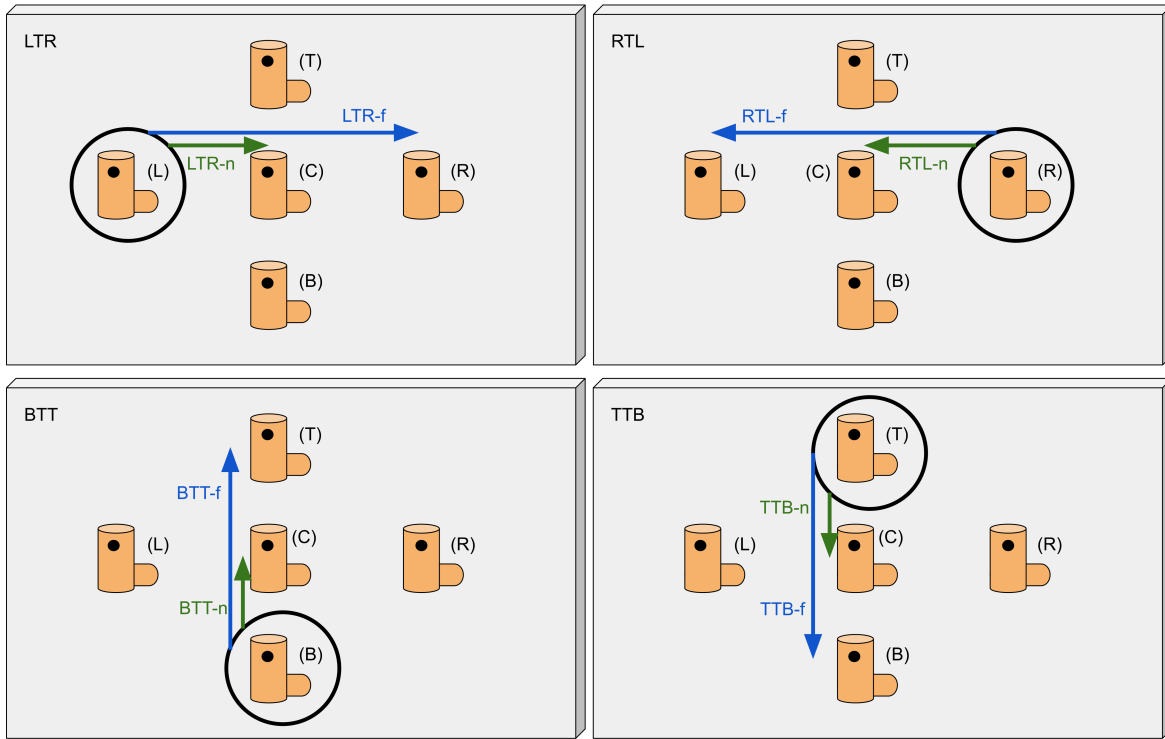


Figure 2.4: Possible trial types. **LTR**: Left-to-right trial with the starting position at the left (L) handle and target positions at the center (C) or right (R) handle, i.e. a LTR-n or LTR-f trial, respectively. **RTL**: Right-to-left trial with the starting position at the right (R) handle and target positions at the center (C) or left (L) handle, i.e. a RTL-n or RTL-f trial, respectively. **BTT**: Bottom-to-top trial with the starting position at the bottom (B) handle and target positions at the center (C) or top (T) handle, i.e. a BTT-n or BTT-f trial, respectively. **TTB**: Top-to-bottom trial with the starting position at the top (T) handle and target positions at the center (C) or bottom (B) handle, i.e. a TBB-n or TBB-f trial, respectively.

2.1.4.2 Eye block

To clean the experiments of eye artifacts later, two blocks of the eye paradigm were performed. One block at the beginning of the experiment and one block in the middle of the experiment. One eye block consisted of 27 trials with four different conditions pseudo-randomly distributed.

Paradigm

Kobler et al. (2020) developed a paradigm for recording eye movements and resting

EEG that can later be used to remove EOG artifacts from contaminated trials [25]. The paradigm was slightly modified from [25] so that no screen was required. Instead, an auditory cue was used to indicate the trial type, and the experiment board handles from section 2.1.3 were used as anchor points.

The four conditions used were horizontal eye movements (HORZ), vertical eye movements (VERT), blinking (BLINK), and rest (REST), as in [25]. For the HORZ and VERT conditions, participants were instructed to move their eyes between the left and right handles and between the bottom and top handles, respectively. The speed of eye movements was at a self-selected pace, with an approximate pace trained before each eye block. During the BLINK trials, subjects were instructed to fixate their gaze on the middle handle and blink their eyes at a self-selected pace, again training an approximate pace before each eye block. During the REST trials, participants fixed their gaze on the middle handle and were instructed to avoid artifacts as much as possible.

Figure 2.5 depicts the eye paradigm. At the beginning, a sound was played indicating the trial type (HORZ, VERT, BLINK, or REST). Then the participants executed the selected condition for 11 seconds, although only the last 10 seconds were taken for analysis. After that period, a beep was played, indicating the end of the trial and starting a break of 2 to 3 seconds.

2.2 Pre-processing

Figure 2.6 displays the pre-processing pipeline performed, adapted from [22]. The pre-processing steps were performed using Python 3.10 (Python Software Foundation, Beaverton, Oregon, USA) and the MNE-Python package version 1.3.1 [26], [27] for processing EEG signals. Additionally, the eye artifact correction algorithm was interfaced using MATLAB (The MathWorks Inc., Natick, Massachusetts, USA) and the distributed algorithm³ from Kobler et al. (2020) [25]. The entire source code for the pre-processing pipeline can be found at <https://github.com/petertumfart/decoding-of-range-EEG>.

³<https://github.com/rkobler/eyeartifactcorrection>

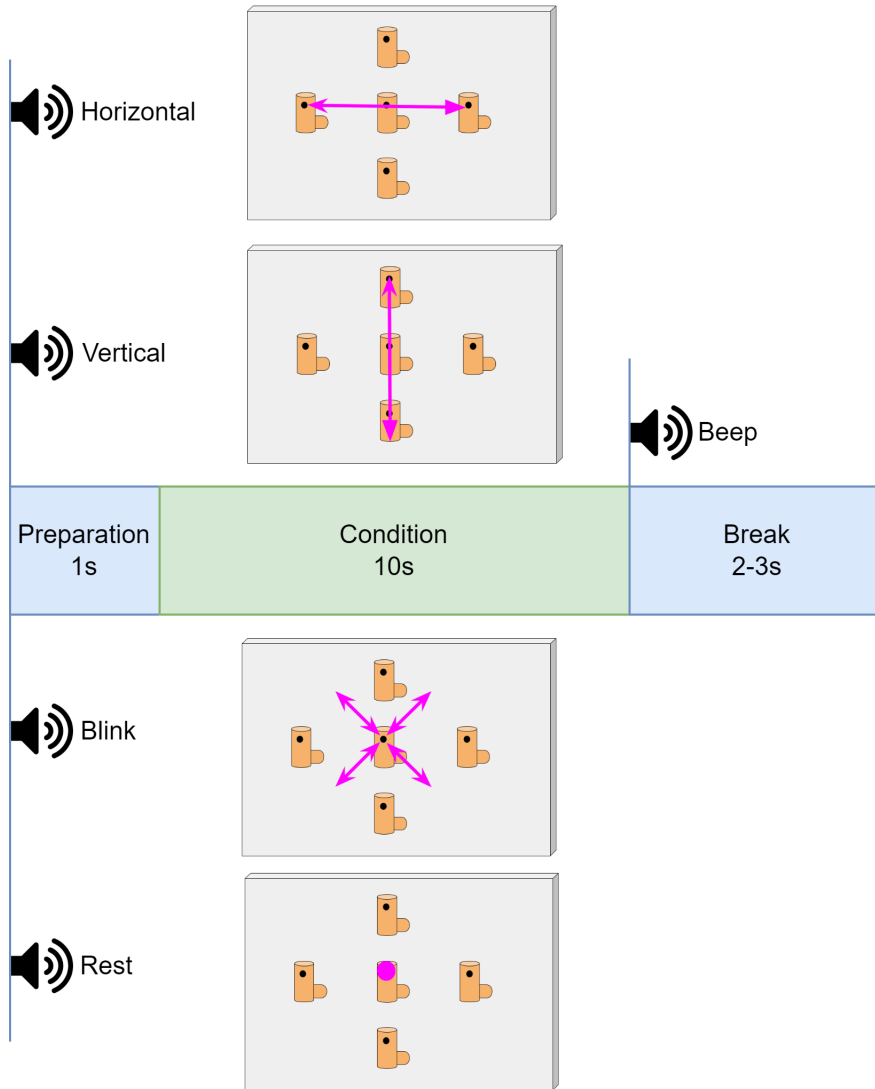


Figure 2.5: Timing of the eye paradigm. The condition is played as a sound at the beginning of the trial and the participants start to execute the condition for 11 seconds. A beep indicates the end of a trial with a break of 2 to 3 seconds.

The raw EEG from the execution paradigm and the raw EEG and EOG signals from the eye paradigm were high-pass filtered with an 8th-order zero-phase Butterworth filter at a cutoff frequency of 0.4 Hz to remove low-frequency artifacts such as sweat or motion artifacts [28]. A notch filter was used to suppress the power line noise. This filter was implemented as a steep band-stop filter (zero-phase Butterworth 16th order) with a lower cutoff frequency of 49.38 Hz and an upper cutoff frequency of 50.62 Hz. Then,

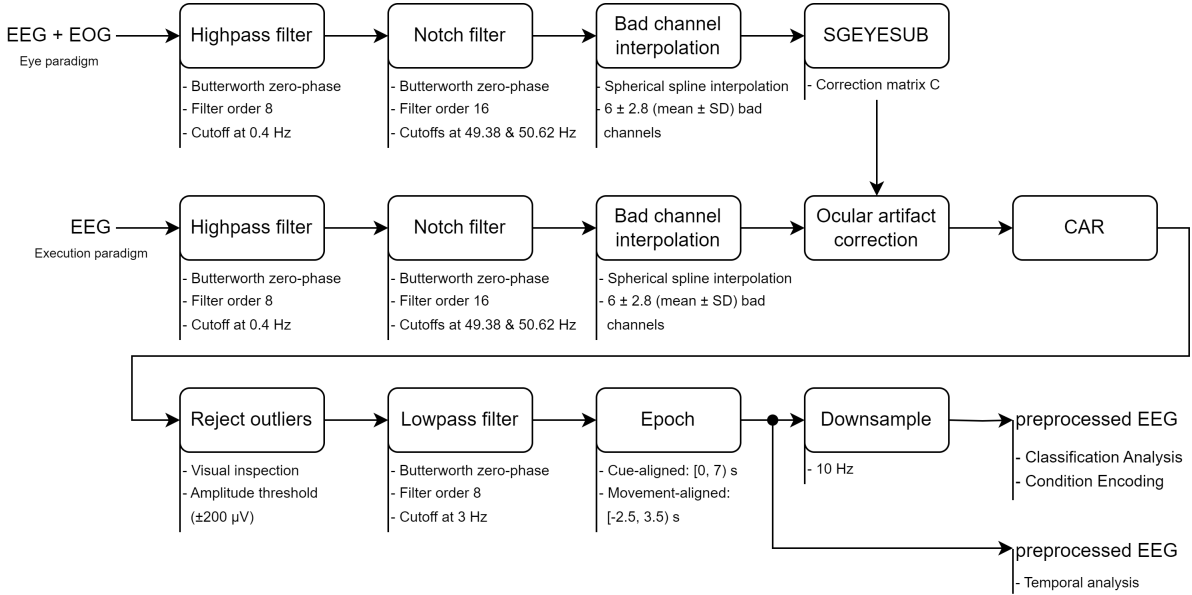


Figure 2.6: Pre-processing steps. The EEG signals from the execution paradigm and the EEG + EOG signals from the eye paradigm were both high-pass filtered at 0.4 Hz and notch filtered at $f_{center} = 50$ Hz. Bad channels were interpolated and the SGEYESUB algorithm was trained for the eye paradigm. This model was then applied to the EEG signals from the execution paradigm. The EEG corrected for eye artifacts was re-referenced to the common average reference. Outliers were removed and a 3.0 Hz low-pass filter was applied. The resulting signal was resampled to 10 Hz and epoched, aligned once to cues and once to movement onsets.

poor channels for each subject were identified by visual inspection and interpolated by spherical splines, 6 ± 2.8 channels (mean \pm standard deviation) were interpolated.

The EEG and EOG signals from the eye paradigm were then fed to the sparse generalized eye artifact subspace subtraction (SGEYESUB) algorithm introduced by Kobler et al. (2020). They have shown that their algorithm performs best in maintaining brain activity while also correcting eye artifacts compared to other eye artifact correction algorithms [25]. When fitted with the data, i.e., the segments for vertical and horizontal eye movements, blinks, and resting activity, the algorithm outputs a $n_{channels} \times n_{channels}$ correction matrix C. This matrix can then be used to correct the EEG signals from eye artifacts of the execution paradigm by a simple matrix multiplication for each time point (i), where $x^{(i)}$ is the $n_{channels} \times 1$ original EEG vector at time point (i) and $x_{corr}^{(i)}$ is the

corrected $n_{\text{channels}} \times 1$ EEG vector at time point (i) (equation 2.1) [25].

$$\mathbf{x}_{\text{corr}}^{(i)} = \mathbf{C} \cdot \mathbf{x}^{(i)} \quad (2.1)$$

The EEG corrected for eye artifacts from the execution paradigm was then re-referenced to the common average reference (CAR). CAR is the subtraction of the average signal across all channels from each channel and reduces spatial biases due to the placement of the reference electrode, in our case, the right mastoid [29].

Outliers were then annotated by visual inspection as well as by an amplitude threshold during valid trials. Data spans marked for rejection by amplitude threshold had to exceed amplitudes of $\pm 200 \mu\text{V}$. On average 79.5 ± 25.6 (mean \pm SD) trials out of 360 trials were rejected per subject.

Then an 8th-order zero-phase Butterworth low pass filter at a cutoff frequency of 3 Hz was applied to obtain a signal that is located in the delta band.

The signals were then epoched in the following two ways:

- (i) Cue-aligned: Epochs were aligned at the appearance of the cues, the starting cue marked as time $t = -2 \text{ s}$ and the target cue marked as time $t = 0 \text{ s}$. The end was marked at $t = 5 \text{ s}$ which was the beginning of the break (beep), i.e., one epoch lasted 7 seconds. This allowed us to investigate the responses associated with movement preparation.
- (ii) Movement-aligned: Here, to investigate neural correlates associated with movement initiation and execution, epochs were aligned with the release of the start handle, i.e., the time at which participants freely decided to move to the target handle. The time $t = 0 \text{ s}$ corresponded to the time when the LDR release marker was sent, and epochs were extracted from 2.5 s before release to 3.5 s after release, resulting in a total time of 6 seconds per epoch.

For the temporal analysis and the graphical representation, these signals were used. For the classification analysis and the coding of the different conditions, the epochs were resampled to 10 Hz.

2.3 Temporal analysis

To extract the participants' movement dynamics and validate the self-paced movement onsets, we extracted the time intervals between

- (i) the cue appearance and the release of the starting handle
- (ii) the cue appearance and the touch of the target handle and
- (iii) the release of the starting handle and the touch of the target handle.

The pre-processed epochs without down-sampling were used for temporal analysis. To investigate the event-related responses, the grand averages were computed for all channels across all subjects. The grand average is defined as the mean response of all subjects (Equation 2.2).

$$A_c = \frac{1}{N} \sum_{k=1}^N A_{ck} \quad (2.2)$$

where A_c is the grand average activity at channel c , A_{ck} is the average activity at channel c for subject k and N is the overall number of subjects.

To investigate potential modulations in amplitude of the MRCPs for the movement-aligned approach and the ERPs at frontal areas associated with movement planning for the cue-aligned approach, grand averages were also calculated for the far and near conditions at channels C1 and Fz, respectively.

95 % confidence intervals were computed for each channel and condition using bootstrapping with 10,000 permutations [30]. To calculate the confidence interval using bootstrapping, the data is re-sampled with replacement for n_{perm} -times and the means are calculated for each sample. Afterwards, the values of the 2.5-th percentile and the 97.5-th percentile of all means are chosen as the 95% confidence interval.

2.3.1 Statistical analysis

To determine significant group-level differences of the time intervals between near and far conditions, a paired two-sided two-sample permutation t-test was performed. Similarly,

paired two-sided two-sample permutation t-tests were computed on the grand average amplitudes of the near and far conditions to determine the time points at which group-level amplitudes were significantly different from each other, using 10,000 permutations and a critical p-value of $p_{\text{crit}} = 0.05$. As described by Nichols et al., permutation tests can be used as non-parametric statistical tests that circumvent the problem of multiple comparisons [31]. Therefore, a difference population is calculated for each time point and then for each permutation, the signs are randomly assigned. The t-statistic for the one-sample t-test is calculated for each of the permutations, and a histogram of all t-statistics is generated. The t-statistics of the original samples are then compared to the histogram [32]. The p-value p is calculated by dividing the number of permutations that yielded a higher t-statistic by the total number of permutations. The same is done for the t-statistics that resulted in a lower t-statistic than the original statistic. Significant differences were then found at time points where the smaller of the two p-values is smaller than half the critical p-value ($p < \frac{p_{\text{crit}}}{2}$).

2.4 Classification analysis

To investigate whether it is possible to distinguish between the different conditions, we trained and evaluated shrinkage linear discriminant analysis (sLDA) classifiers for the conditions of interest.

2.4.1 Linear discriminant analysis (LDA)

The multi-class LDA and therefore the two-class LDA for the number of classes $K = 2$ can be derived from a probabilistic approach using the Bayes theorem (Eq. 2.3).

$$p(C_k|\mathbf{x}) = \frac{p(\mathbf{x}|C_k)p(C_k)}{\sum_{j=1}^K p(\mathbf{x}|C_j)} \quad (2.3)$$

Where k is the class of interest, K is the number of classes, $p(C_k|\mathbf{x})$ denotes the posterior probability that a sample \mathbf{x} belongs to class C_k , $p(\mathbf{x}|C_k)$ is the likelihood

probability that a sample \mathbf{x} is observed given a class C_k , $p(C_k)$ being the a-priori probability of a class C_k , and the denominator being the marginalization term as the sum of all likelihoods.

For LDA the likelihood for a class C_k follows a Gaussian distribution given as

$$p(\mathbf{x}|C_k) = \frac{1}{(2\pi)^{D/2}|\widehat{\Sigma}_k|^{1/2}} \exp\left(-\frac{1}{2}(\mathbf{x} - \boldsymbol{\mu}_k)^T \widehat{\Sigma}_k^{-1} (\mathbf{x} - \boldsymbol{\mu}_k)\right). \quad (2.4)$$

With D being the number of features, $\widehat{\Sigma}_k$ being the sample covariance matrices for each class and $\boldsymbol{\mu}_k$ being the class means.

With the assumption that all classes have the same empirical covariance matrix $\widehat{\Sigma}$, the log-posterior distribution follows as

$$\ln(p(C_k|\mathbf{x})) = -\frac{1}{2}(\mathbf{x} - \boldsymbol{\mu}_k)^T \widehat{\Sigma}^{-1} (\mathbf{x} - \boldsymbol{\mu}_k) + \ln(p(C_k)). \quad (2.5)$$

with

$$\widehat{\Sigma} = \frac{1}{n_{\text{samples}}} \mathbf{x} \mathbf{x}^T \quad (2.6)$$

Which can be factorized into

$$\ln(p(C_k|\mathbf{x})) = \mathbf{w}_k \mathbf{x} + w_{k0} \quad (2.7)$$

with

$$\mathbf{w}_k = \widehat{\Sigma}^{-1} \boldsymbol{\mu}_k \quad (2.8)$$

$$w_{k0} = -\frac{1}{2} \boldsymbol{\mu}_k^T \widehat{\Sigma}^{-1} \boldsymbol{\mu}_k + \ln(p(C_k)). \quad (2.9)$$

With \mathbf{w}_k being the weight vector and w_{k0} being the bias or intercept term [33].

Finally, the decision is made by choosing the class with the highest log-posterior probability, i.e.

$$k_{\text{predict}} = \arg \max_k \ln(p(C_k|\mathbf{x})). \quad (2.10)$$

The two assumptions made, that the classes follow Gaussian distributions and that the classes have the same covariance matrix, are valid assumptions for ERP signals, as

shown by Blankertz et al. [34].

2.4.1.1 Shrinkage LDA (sLDA)

When the number of features compared to the number of samples is high, then the model may not generalize well to unseen data. To tackle this problem, shrinkage can be used in the estimation of the covariance matrix in the form of

$$\widehat{\Sigma}^* = (1 - \alpha)\widehat{\Sigma} + \alpha \frac{\text{Tr}(\widehat{\Sigma})}{D} \mathbf{I}. \quad (2.11)$$

Where D is the number of features, \mathbf{I} the identity matrix, and α a shrinkage factor between 0 and 1 determining the amount of regularization, with $\alpha = 0$ no regularization and $\alpha = 1$ leading to an isotropic covariance matrix [34].

This shrinkage parameter was estimated using the lemma of Ledoit and Wolf, which provides an explicit formula to find the optimal shrinkage parameter α [35].

2.4.2 Application of sLDA

To investigate the time course of the classification results, sLDA classifiers were fitted and evaluated for each time point of the pre-processed and down-sampled EEG.

2.4.2.1 Features

Each classifier was trained and evaluated with two sets of features:

1. **Single time point features:** The features were the EEG signals from all channels at the current time point, resulting in $D = 61$ features to obtain a responsive estimate of classification accuracy over time.
2. **Window-based approach** The features were the EEG signals from all channels at the current time point plus five previous time points, resulting in $D = 61 \cdot 6 = 366$ features. This approach is expected to deliver more sustained classification results [22].

2.4.2.2 Conditions

In total we had 5 conditions with different numbers of classes.

- (i) **Range classifier:** A two-class classifier separating the near and far movements. That means trials LTR-n, RTL-n, BBT-n, and TTB-n were marked as the *near* class and trials LTR-f, RTL-f, BBT-f, and TTB-f were marked as the *far* class.
- (ii) **Direction classifier:** A four-class classifier separating all directions, regardless of distance. Trials LTR-n and LTR-f marked class *right*, trials RTL-n and RTL-f marked class *left*, trials BTT-n and BTT-f marked class *up*, and trials TTB-n and TTB-f marked class *down*.
- (iii) **Near direction classifier:** A four-class classifier separating all directions, but only taking near trials into account. Trials LTR-n marked class *right-near*, trials RTL-n marked class *left-near*, trials BTT-n marked class *up-near*, and trials TTB-n marked class *down-near*.
- (iv) **Far direction classifier:** A four-class classifier separating all directions, but only taking far trials into account. Trials LTR-f marked class *right-far*, trials RTL-f marked class *left-far*, trials BTT-f marked class *up-far*, and trials TTB-f marked class *down-far*.
- (v) **Position classifier:** A five-class classifier separating all target positions. Trials LTR-f marked class *right-pos*, trials RTL-f marked class *left-pos*, trials BTT-f marked class *top-pos*, trials TTB-f marked class *bottom-pos* and trials LTR-n, RTL-n, BBT-n, and TTB-n marked class *center-pos*.

For each classifier, the number of trials for each class was equalized to obtain balanced class sample sizes, as sLDA would be unlikely to identify the minority class [36], [37]. This is especially important for the position classifier (v), where the center class would account for half of the trials, while the other classes would represent only one-eighth of the trials.

2.4.2.3 Evaluation

Each classifier was evaluated in a Leave-one-out (LOO) cross-validation (CV) scheme (see Figure 2.7) for each participant. In this special form of k-fold cross validation, the dataset of length n_{trials} is split into a training set of size $n_{\text{trials}} - 1$ and tested on the held-out sample. This was repeated for n_{trials} -times such that each trial was once in the held-out set, leading to n_{trials} test accuracies. This technique is computationally expensive but yields an estimate of accuracy that is not as biased as k-fold cross-validation, especially when data are scarce [33].

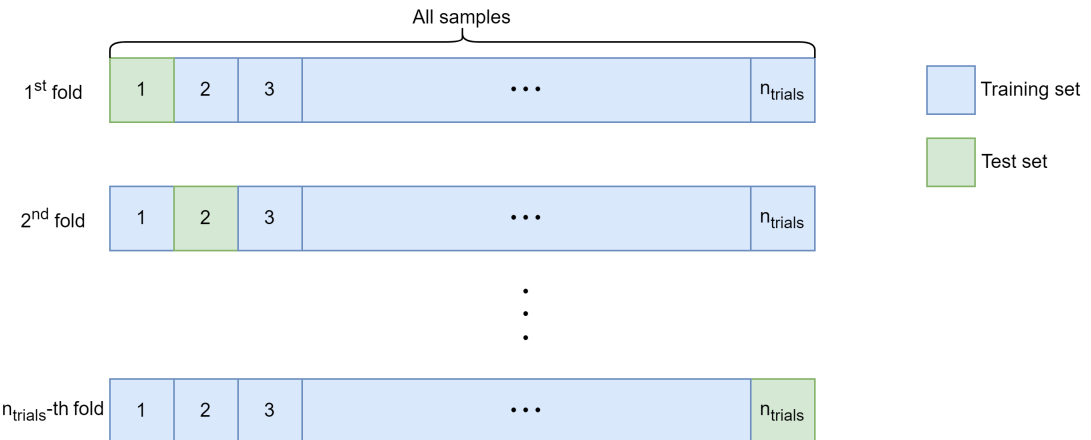


Figure 2.7: Leave-one-out cross-validation (LOO-CV) scheme. Each square represents a sample. In the first set, the first sample is taken out and used as the test set, while the remaining samples form the training set. In the next iteration, the second sample is retained as the test set, while the remaining samples form the training set. This procedure is repeated n_{trials} times so that each sample is used once as the test set.

The mean test accuracy for each subject is then used to compute the grand average accuracy for all participants for each time-point (Eq. 2.12).

$$\text{acc} = \frac{1}{n_{\text{trials}}} \sum_{i=1}^{n_{\text{trials}}} \text{acc}_i \quad (2.12)$$

Additionally, an average confusion matrix was calculated by averaging the subject confusion matrices calculated at the time point of peak accuracy for each subject. For the direction and position classifiers in the cue-aligned approach, confusion matrices

were also calculated for the time period prior to the target cue.

To determine the true chance level, which deviates from the theoretical chance level because of a finite number of trials [38], a permutation method following Combrisson et al. was chosen [39]. Here, class labels were randomly assigned to the samples and the LOO evaluation procedure was repeated 10,000 times, leading to a null distribution. The upper tail of this null distribution, i.e., the 95 percentile of the mean test accuracies, was chosen as the significance level for each classifier. The 95th-percentile corresponds to an alpha value of $\alpha = 0.05$. This procedure was repeated for each participant and the mean chance level is reported in the results.

2.4.2.4 Statistical analysis

A one-sample one-tailed permutation t-test was used to determine the time points at which group-level accuracies were significantly different from the chance level, using 10,000 permutations and a critical p-value of $p_{\text{crit}} = 0.05$. The one-sample permutation t-test is calculated similarly to that described in section 2.3.1, with the distinction that a group mean, in this case the chance level, is subtracted from the subjects accuracies.

2.5 Encoding of distance and direction/position

To investigate possible differences between the different conditions on a topographic level and to find regions that contribute to movement preparation and execution, a general linear model (GLM) was used to encode the different conditions [22], [40].

2.5.1 General linear model (GLM)

The GLM can be stated as:

$$\mathbf{X}^{(i)} = \Phi \boldsymbol{\Theta}^{(i)} + \boldsymbol{\epsilon}^{(i)}. \quad (2.13)$$

Where $\mathbf{X}^{(i)}$ is called the response matrix, a $n_{\text{trials}} \times n_{\text{channels}}$ matrix containing the pre-processed EEG at time point i , Φ is a $n_{\text{trials}} \times n_{\text{conditions}}$ design matrix containing the encoded factors for the conditions, $\Theta^{(i)}$ is a $n_{\text{conditions}} \times n_{\text{channels}}$ coefficient matrix containing the regression coefficients at time point i , and $\epsilon^{(i)}$ is a $n_{\text{trials}} \times n_{\text{channels}}$ matrix containing the remaining data that cannot be explained by the factors at time point i .

There were 5 conditions to be encoded in the GLM, namely *near*, *far*, *horizontal*, *vertical* and *intercept*. These conditions are encoded in the design matrix Φ by assigning each trial k a condition vector φ_k which contains the conditions:

$$\varphi_k = [c_{\text{near}} \quad c_{\text{far}} \quad c_{\text{horizontal}} \quad c_{\text{vertical}} \quad 1]. \quad (2.14)$$

Where each factor c is either 0 or 1 depending on the trial type. Stacking the row vectors for all trials leads then to the design matrix Φ :

$$\Phi = \begin{bmatrix} \varphi_1 \\ \vdots \\ \varphi_k \\ \vdots \\ \varphi_{n_{\text{trials}}} \end{bmatrix}. \quad (2.15)$$

Each column of the design matrix, besides the intercept term, was then standardized to obtain zero mean and a standard deviation of one (Eq 2.16).

$$c_{\text{standardized}} = \frac{c - \text{mean}(c)}{\text{std}(c)} \quad (2.16)$$

The coefficient matrix can then be obtained using linear regression and the regularized least squares solution (RLS).

Equation 2.13 solved for the coefficient matrix $\Theta^{(i)}$ at time point i , using the ordinary least squares (OLS) solution, results in

$$\widehat{\Theta}^{(i)} = (\Phi^T \Phi)^{-1} \Phi^T \mathbf{X}^{(i)}. \quad (2.17)$$

With the empirical covariance matrix $\widehat{\Sigma} = \frac{1}{n}\Phi^T\Phi$, equation 2.17 can be re-written as

$$\widehat{\Theta}^{(i)} = \frac{1}{n} \left(\frac{1}{n} \Phi^T \Phi \right)^{-1} \Phi^T \mathbf{X}^{(i)} = \frac{1}{n} \widehat{\Sigma}^{-1} \Phi^T \mathbf{X}^{(i)} \quad (2.18)$$

As in section 2.4.1.1, regularization is introduced via the sample covariance matrix $\widehat{\Sigma}$, where the shrunken covariance matrix $\widehat{\Sigma}^*$ is estimated using Ledoit and Wolf's lemma [35]. This ultimately leads to the regression coefficients at each time point, as follows:

$$\widehat{\Theta}^{(i)} = \frac{1}{n} \widehat{\Sigma}^{*-1} \Phi^T \mathbf{X}^{(i)}. \quad (2.19)$$

The explained EEG by the regression coefficients can then be estimated as:

$$\widehat{\mathbf{X}}^{(i)} = \Phi \widehat{\Theta}^{(i)} \quad (2.20)$$

The residual noise at each time point can then be estimated as:

$$\epsilon^{(i)} = \mathbf{X}^{(i)} - \widehat{\mathbf{X}}^{(i)} \quad (2.21)$$

2.5.1.1 Statistical analysis

To determine which brain regions encode the range and direction parameters, one-sample two-sided permutation t-tests (in the same fashion as explained in section 2.3.1) were performed for each element of the regression parameter matrix $\widehat{\Theta}^{(i)}$ and each time point i with 10,000 subject-level permutations against a group mean of 0. Channels with significant differences from zero ($p_{\text{crit}} = 0.05$) were then remapped to the EEG activity on a topographic representation.

To compare for differences in the range conditions (near vs. far) and in the direction conditions (vert vs. horz) two-sample permutation t-tests ($n_{\text{perm}} = 10,000$) were performed on the regression coefficients and re-mapped to the topoplots where significant differences were found ($p_{\text{crit}} = 0.05$). The same test was applied for range vs. direction. Here, the far and near encoded regression coefficients were tested against the horizontal

and vertical encoded coefficients.

3 Results

The results chapter presents the findings of the work, highlighting the main results and statistical relevance of the analyses performed.

3.1 Temporal results

3.1.1 Movement timings

The box plots in Figure 3.1 illustrate the timing differences between cue presentation and releasing the starting handle (left), cue presentation and touching the target handle (middle) and the difference between releasing the starting handle and touching the target handle (right) for near (red) and far (blue) distances. The average duration between seeing the cue and releasing the starting handle was $1.41 \text{ s} \pm 0.41 \text{ s}$ (mean \pm SD) for near trials and $1.38 \text{ s} \pm 0.42 \text{ s}$ (mean \pm SD) for far trials, showing no significant differences between the two conditions ($p\text{-value} = 0.1216$, two-sided paired permutation t-test with 10,000 permutations, $p_{\text{crit}} = 0.05$). The difference between presenting the cue and the subjects touching the target handle was $2.20 \text{ s} \pm 0.55 \text{ s}$ (mean \pm SD) for near trials and $2.29 \text{ s} \pm 0.57 \text{ s}$ (mean \pm SD) for far trials and a $p\text{-value}$ of 0.0972 (two-sided paired permutation t-test with 10,000 permutations, $p_{\text{crit}} = 0.05$). Finally, the difference between releasing the starting handle and touching the target handle was $0.78 \text{ s} \pm 0.16 \text{ s}$ (mean \pm SD) for near trials and $0.91 \text{ s} \pm 0.17 \text{ s}$ (mean \pm SD) for far trials, showing significant differences ($p\text{-value} = 0.0038$, two-sided paired permutation t-test with 10,000 permutations, $p_{\text{crit}} = 0.05$).

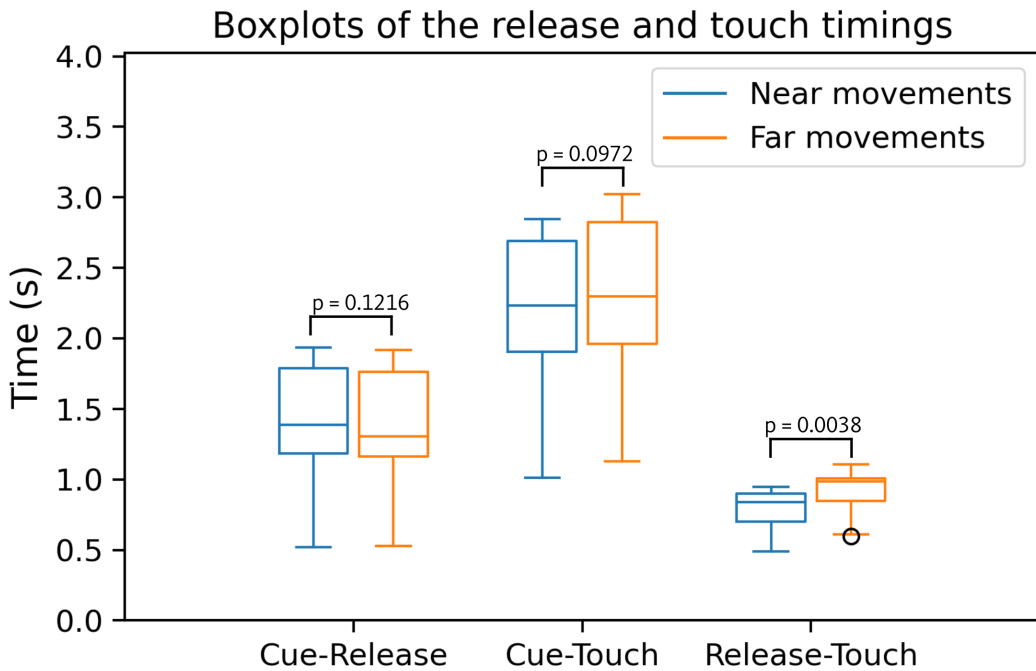


Figure 3.1: Box plots of the movement timings. Left: Duration between cue presentation and releasing the starting handle for near (red, left) and far (blue, right) trials. Middle: Duration between cue presentation and touching the target handle for near (red, left) and far (blue, right) trials. Right: Duration between releasing the starting handle and touching the target handle for near (red, left) and far (blue, right) trials.

3.1.2 Grand average results

The following results show the grand average results for the two different epoching methods, cue-aligned and movement-aligned.

3.1.2.1 Cue-aligned

The grand average activity on channel C1 shows an initial small positivity of about $1 \mu\text{V}$ at time $t = -1.7 \text{ s}$ subsequent to the start handle cue at time $t = -2 \text{ s}$, followed by a strong negativity of about $-2 \mu\text{V}$ at time $t = -1.1 \text{ s}$, before returning to the initial value preceding the presentation of the target cue at time $t = 0 \text{ s}$, with a small overshoot at $t = -0.5 \text{ s}$ for both, the near and far trials (Fig. 3.2 A). After presentation of the target cue at $t = 0 \text{ s}$, the EEG shows a small positivity of about $0.9 \mu\text{V}$ after 0.3 s , followed by

a small negativity of about $-0.9 \mu\text{V}$ at $t = 0.9 \text{ s}$, revealing significant differences between near and far trials at durations $0.02 \text{ s} - 0.09 \text{ s}$, $0.39 \text{ s} - 0.52 \text{ s}$, and $0.66 \text{ s} - 0.77 \text{ s}$ (two-sided paired permutation t-tests with 10,000 permutations) (Fig. 3.2 **A**, lime bars mark significant differences). Afterwards, the activity returns to the baseline with a significant difference at time span $2.3 \text{ s} - 2.42 \text{ s}$ (Fig. 3.2 **A**).

The grand average activity on channel Fz is shown in Figure 3.2 **B**. The activity starts with a positivity peaking at about $1.5 \mu\text{V}$ at $t = -1.9 \text{ s}$ followed by a steep negative shift to around $-1.5 \mu\text{V}$ at $t = -1.5 \text{ s}$ and slowly rises to baseline towards $t = 0 \text{ s}$ (Fig. 3.2 **B**). After the target cue presentation at $t = 0 \text{ s}$, the EEG shows a positive peak of around $1 \mu\text{V}$ at $t = 0.2 \text{ s}$ followed by a negativity of about $-0.7 \mu\text{V}$ at $t = 0.4 \text{ s}$ and then returning to the baseline until the end of the trial (Fig. 3.2 **B**). Significant differences could be found at durations $-1.03 \text{ s} - 0.86 \text{ s}$, $t = 0.0 \text{ s} - 0.08 \text{ s}$, $t = 0.4 \text{ s} - 0.54 \text{ s}$, $t = 0.68 \text{ s} - 0.84 \text{ s}$, $t = 2.04 \text{ s} - 2.22 \text{ s}$, $t = 2.42 \text{ s} - 2.48 \text{ s}$ and $t = 2.95 \text{ s} - 3.0 \text{ s}$ using a two-sided paired permutation t-test with 10,000 permutations (Fig. 3.2 **B**, lime bars mark significant differences).

The smoothed histogram of the movement timings is displayed at the top of Figure 3.2 **A** as well as at the top of Figure 3.2 **B** to achieve a better visual assignment of the motion sequences to the EEG signals. The pink line depicts the durations from the presentation of the target cue until the movement onset, i.e., release of the starting handle and the gray line indicates the durations from the presentation of the target cue to the grasp of the target handle.

Figure 3.2 **C** shows the topoplots at distinct time points from $t = 0 \text{ s}$ to $t = 3.9 \text{ s}$ in 0.1 s steps for both conditions combined, the near and far trials. The topoplots reveal a positivity on fronto-central channels at $t = 0.3 \text{ s}$ and a negativity at $t = 0.4 \text{ s}$ on parieto-occipital channels reflecting the visual evoked potential (VEP) due to the cue presentation at the target handle.

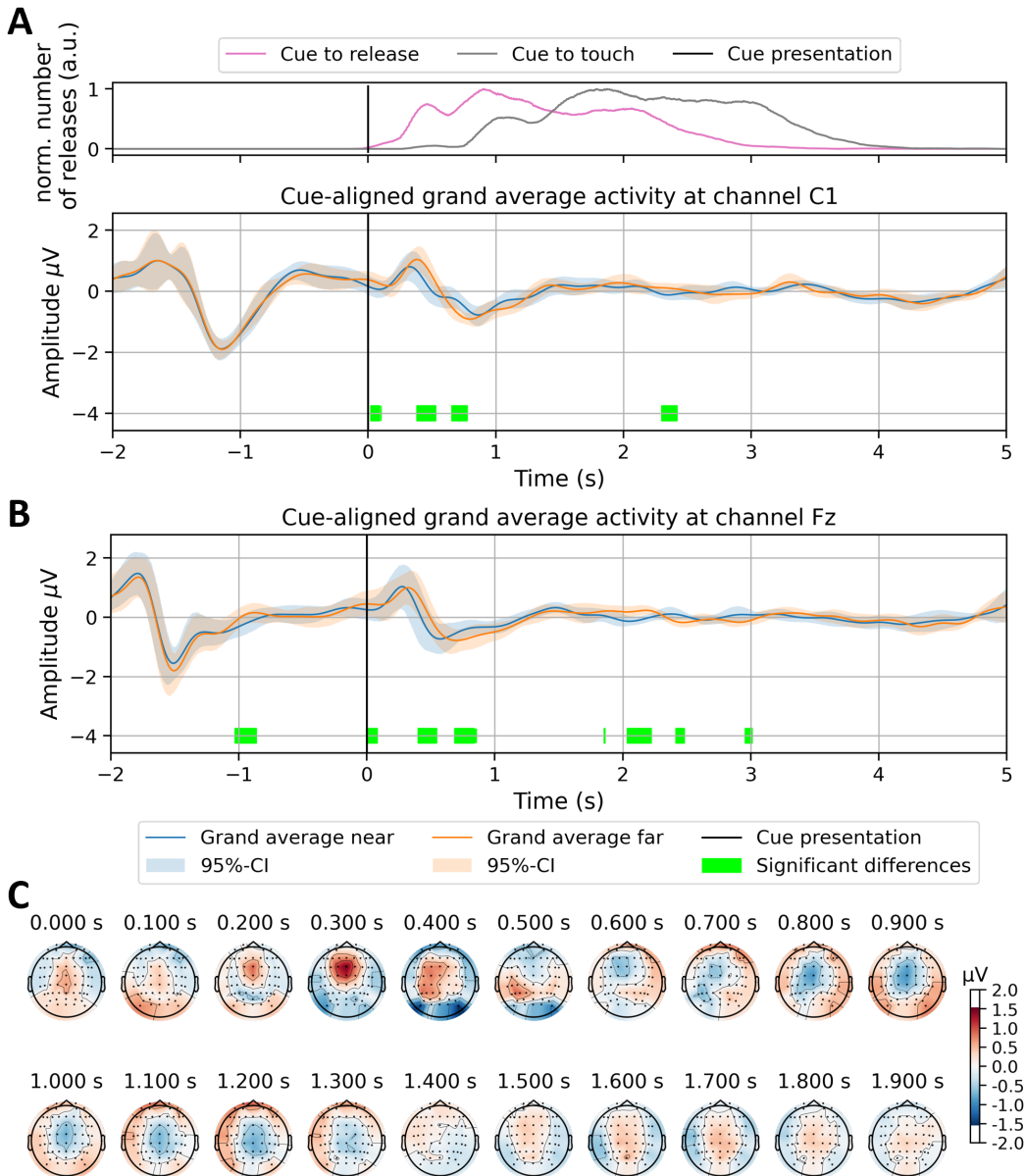


Figure 3.2: Grand average results for cue-aligned epoching. **A:** Top: Smoothed histogram of the release (pink) and touch (gray) durations w.r.t. the cue presentation. Bottom: Grand average results at channel C1 for near trials (blue) and for far trials (orange) together with 95% confidence intervals (shaded areas). Lime bars in the bottom highlight time points with significant differences (paired two-sided permutation t-test, 10,000 permutations and $p_{crit} = 0.05$). **B:** Same as for **A** but for channel Fz. **C:** Topoplots for distinct time points around the cue presentation from 0 s to 1.9 s in 0.1 s steps.

3.1.2.2 Movement-aligned

Similar to the cue-aligned grand average results, we looked at the grand average results when epoching was performed aligned to the movement onset, i.e., the release of the starting handle marking time point $t = 0\text{ s}$. The grand average activity on channel C1 oscillates around $0\text{ }\mu\text{V}$ from $t = -2.5\text{ s}$ until about $t = -1.3\text{ s}$ (Fig. 3.3 **A**). Then, a slow positive shift from $t = -1.3\text{ s}$ until $t = -0.3\text{ s}$ peaking at about $0.5\text{ }\mu\text{V}$ follows prior to the movement onset (Fig. 3.3 **A**). Afterwards, an oscillation around the movement onset can be observed, with a negative peak of $-1.1\text{ }\mu\text{V}$ at $t = -0.1\text{ s}$, a positive peak of $0.5\text{ }\mu\text{V}$ at $t = 0.07\text{ s}$, again a negativity of about $-1.1\text{ }\mu\text{V}$ at $t = 0.3\text{ s}$ and finally a positive plateau of $0.8\text{ }\mu\text{V}$ from $t = 0.7\text{ s}$ to $t = 1.3\text{ s}$ before returning to the baseline (Fig. 3.3 **A**). Significant differences between the two conditions could be found during the oscillation after the movement onset from $t = 0.16\text{ s}$ to $t = 0.25\text{ s}$ and at the last positive plateau from $t = 1.18\text{ s}$ to $t = 1.27\text{ s}$, where the plateau for far trials lasts a little longer (two-sided paired permutation t-tests with 10,000 permutations) (Fig. 3.3 **A**, bottom, lime bars mark significant differences). Further, significant differences could be found towards the end of the trial from $t = 2.29\text{ s}$ to $t = 2.44\text{ s}$ and $t = 2.96\text{ s}$ to $t = 3.04\text{ s}$.

The grand average activity on channel Fz is shown in Figure 3.3 **B**. The EEG oscillates around the baseline until $t = -0.4\text{ s}$ which marks the begin of an oscillation around the movement-onset (Fig. 3.3 **B**). It starts with a negativity of around $-2\text{ }\mu\text{V}$ followed by a positive peak of $1\text{ }\mu\text{V}$ at $t = 0.1\text{ s}$, afterwards, a negativity of about $-0.5\text{ }\mu\text{V}$ at $t = 0.5\text{ s}$ follows, marking the end of the oscillation before the signal returns to the baseline with a small overshoot (Fig. 3.3 **B**). Significant differences were revealed before the movement onset at durations -1.74 s to -1.7 s and from -0.49 s to -0.34 s (two-sided paired permutation t-tests with 10,000 permutations) (Fig. 3.3 **B**, lime bars mark significant differences). Similar to the cue-aligned approach, the smoothed histogram of the movement timings is displayed at the top of Figure 3.3 **A** as well as at the top of Figure 3.3 **B** but aligned to the movement onset. The pink line depicts the durations from the release of the starting handle until the presentation of the target cue (looking

backwards) and the gray line indicates the durations from the release of the starting handle to the grasp of the target handle.

Figure 3.3 **C** shows the topoplots at distinct time points from $t = -1.0\text{ s}$ to $t = 0.9\text{ s}$ in 0.1 s steps for both conditions combined, the near and far trials. The topoplots show a strong negativity on fronto-central channels and a positivity on parieto-occipital channel at $t = -0.1\text{ s}$ and a latter negativity on central channels for time points $t = 0.3\text{ s}$ and $t = 0.4\text{ s}$.

3.2 Classification results

To assess the ability to distinguish between the different conditions, range, direction and position, the results of the applied sLDA classifiers are presented in the following subsections.

3.2.1 Range classifier

3.2.1.1 Cue-aligned

Figure 3.4 shows the classification results for the 2-class sLDA classifier used to separate the far and near trials using the cue-aligned approach. Similar to the temporal results, the smoothed movement onsets and stops with respect to the presentation of the target cue are shown in Fig. 3.4 **A**. The evolution of the classification accuracy for the window-based (6 time points) classification approach peaks at time point 0.8 s with an accuracy of 0.64, with significant group level differences from chance level (0.562) ranging from 0.4 s to 0.9 s using one-sided, one-sample permutation t-tests for each time point with 10,000 permutations against a group mean of 0.562, which is the estimated chance level for the two classes (Fig. 3.4 **B**). The average confusion matrix for the peak accuracy for each subject shows a balanced prediction with $32.6\% \pm 3.2\%$ (mean \pm SD) correctly predicted far trials and $32.0\% \pm 3.3\%$ (mean \pm SD) correctly predicted near trials (Fig. 3.4 **C**). The mean accuracy for the single time point approach peaked at 0.61 at time point 2.4 s , showing no significant differences from chance level (0.562) using the

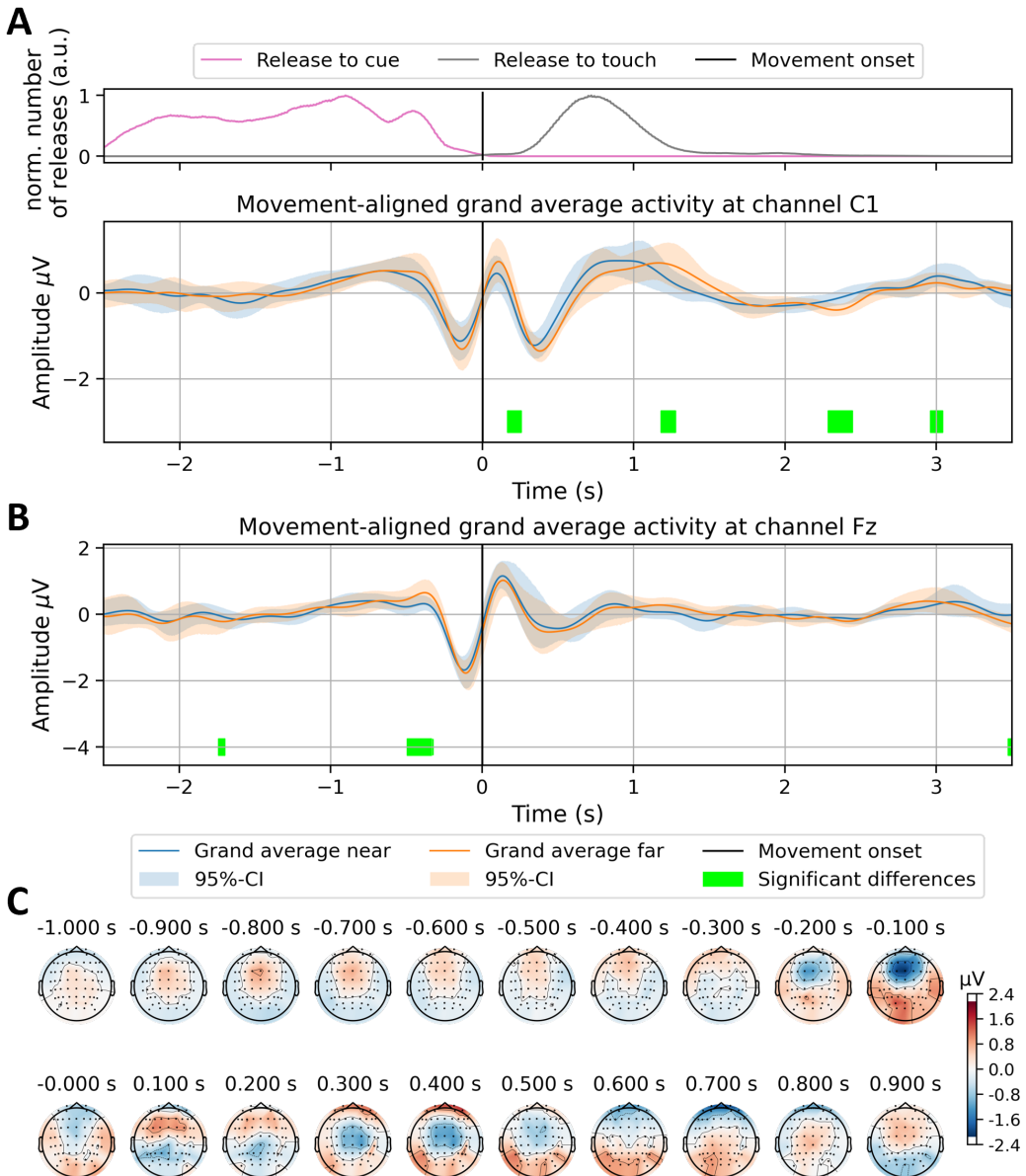


Figure 3.3: Grand average results for movement-aligned epoching. **A:** Top: Smoothed histogram of the cue-presentations (pink) and touches of the target handle (gray) durations w.r.t. the movement onsets, i.e. releases of the starting handle. Bottom: Grand average results at channel C1 for near trials (blue) and for far trials (orange) together with 95% confidence intervals (shaded areas). Lime bars in the bottom highlight time points with significant differences (paired two-sided permutation t-test, 10,000 permutations and $p_{\text{crit}} = 0.05$). **B:** Same as for **A** but for channel Fz. **C:** Topoplots for distinct time points around the movement onset from -1 s to 0.9 s in 0.1 s steps.

same procedure as for the window-based approach (Fig. 3.4 **D**). The average confusion matrix shows a balanced prediction as well, with a slightly lower prediction accuracy of $32.1\% \pm 3.0\%$ (mean \pm SD) and $30.9\% \pm 3.4\%$ (mean \pm SD) for far and near trials, respectively (Fig. 3.4 **E**).

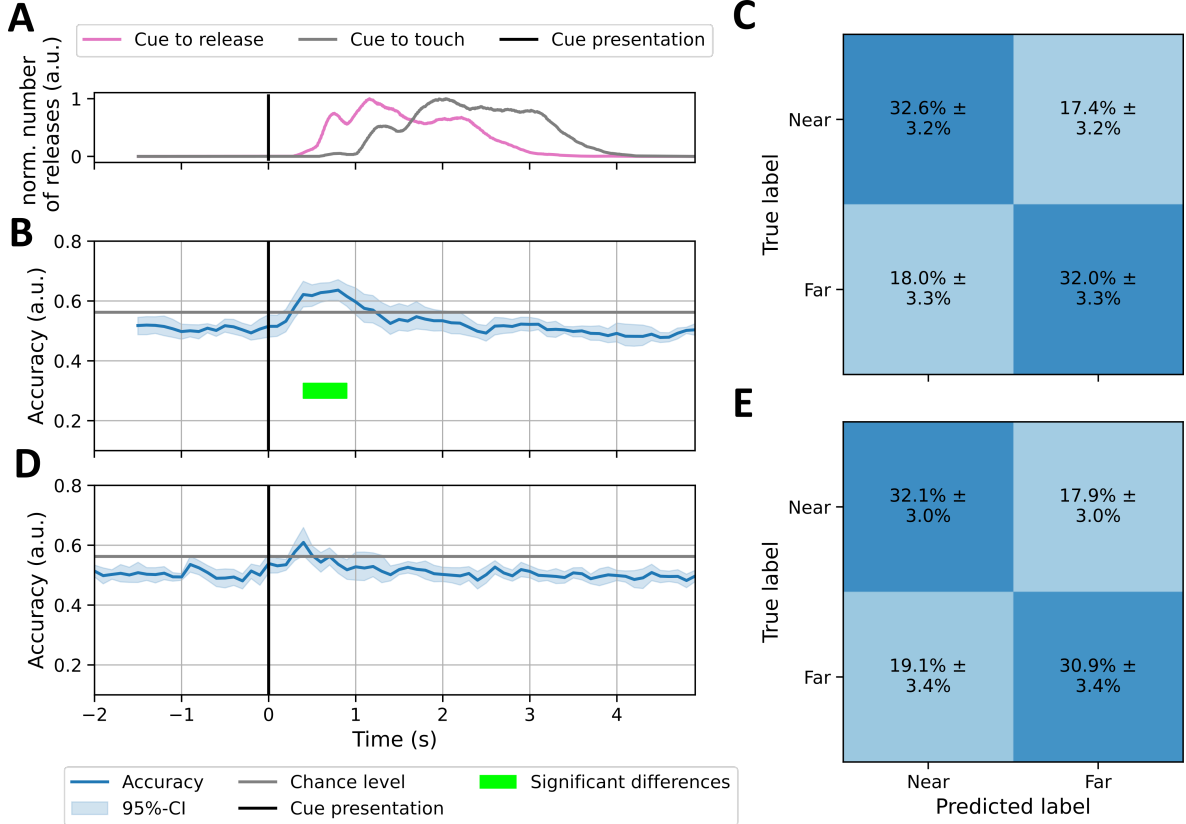


Figure 3.4: Range classification cue-aligned. **A:** Smoothed histogram of the release (pink) and touch (gray) durations w.r.t. the cue presentation. **B:** Classification accuracy for the range classifier using a window of 6 time points (blue) with the 95% confidence interval (shaded area) and the estimated chance level (grey). Lime bars indicate significant differences from the group level accuracy compared to the chance level (one-sided one-sample permutation t-test with 10,000 repetitions, $p_{crit} = 0.05$). **C:** Confusion matrix showing the predicted labels on the x-axis and the true labels on the y-axis for the peak accuracy of each subject between $t = 0$ s and $t = 1.5$ s. **D** and **E**, as in **B** and **C** but for single time point classification.

3.2.1.2 Movement-aligned

The same classification results for the 2-class sLDA as in Fig. 3.4 but for the movement-aligned approach are depicted in Figure 3.5. Around the movement onset ($t = 0$ s), the average classification accuracy for the windowed approach rises from chance level (0.561) and peaks at time 1.1 s with an accuracy of 0.69 and significant differences from chance level were found in the range from 0.2 s to 1.6 s (lime bar, one-sided one-sample permutation t-tests, $n=10,000$, $p_{crit} = 0.05$) (Figure 3.5 **B**). The accuracy evolution for the single time point classifier shows a similar curse peaking at $t = 0.8$ s with an accuracy of 0.63 and a shorter duration of significant differences ranging from $t = 0.5$ s to $t = 1.2$ s (lime bar, one-sided one-sample permutation t-tests, $n=10,000$, $p_{crit} = 0.05$) (Figure 3.5 **D**). The average confusion matrices for the windowed approach and the single time point approach for the peak accuracies of each subject (Fig. 3.5 **C** and **E**, respectively) show similar results, classifying $35.3\% \pm 4.5\%$ (mean \pm SD) of the far trials and $34.7\% \pm 4.0\%$ (mean \pm SD) of the near trials correctly for the windowed approach and classifying $34.0\% \pm 3.8\%$ (mean \pm SD) of the far trials and $34.0\% \pm 3.9\%$ (mean \pm SD) of the near trials correctly for the single time point approach.

3.2.2 Direction classifier

3.2.2.1 Cue-aligned

Figure 3.6 shows the classification results for the direction classifier using far and near trials combined for training and testing in the cue-aligned setting. Again, to align the accuracies to the starts and stops of the movements, the smoothed histogram of movement release (pink) and the touch of the target handle (grey) w.r.t. to the target cue presentation at $t = 0$ s are depicted in Figure 3.6 **A**. The accuracy curve for the windowed approach shows significant group level differences from chance level, which was estimated to be 0.304 for this classifier, prior to the target cue presentation in a window from $t = -1.5$ s to $t = -0.7$ s (lime bar, one-sided one-sample permutation t-tests, $n=10,000$, $p_{crit} = 0.05$) with a peak accuracy of 0.41 at time point $t = -1.2$ s before declining

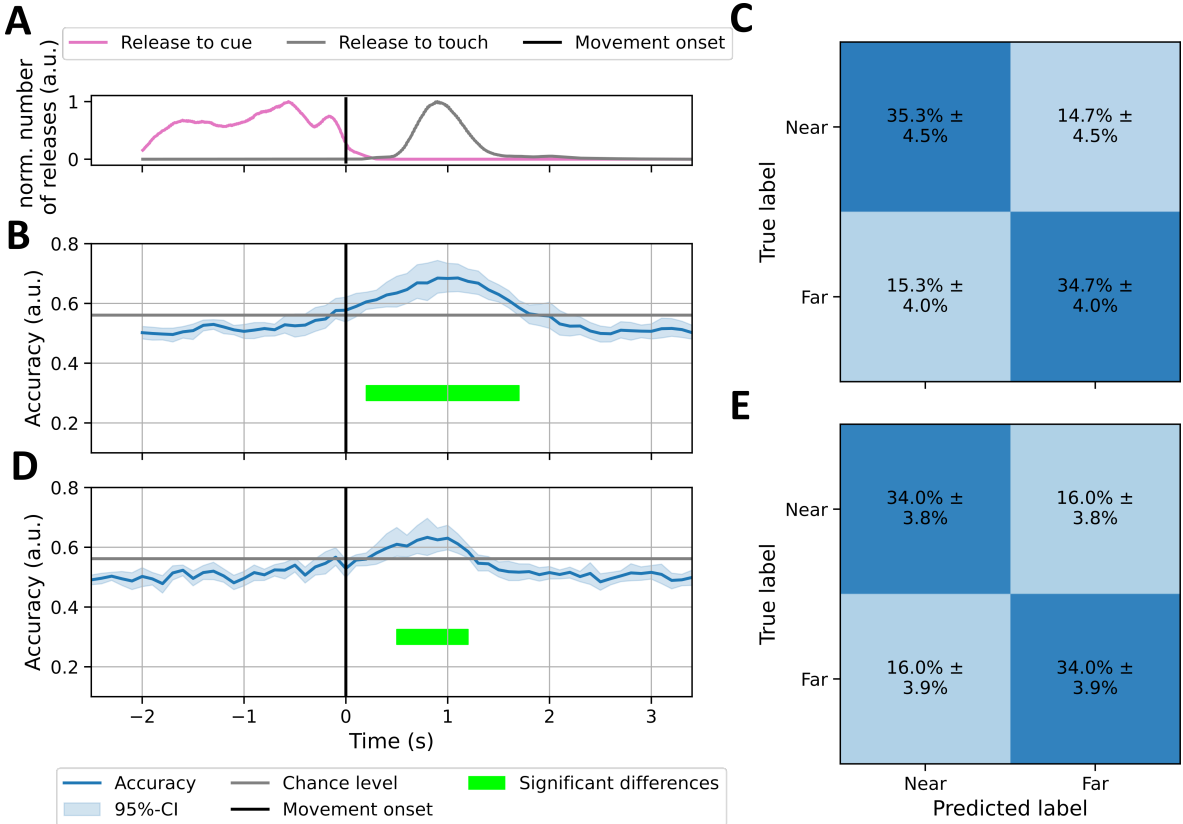


Figure 3.5: Range classification movement-aligned. **A:** Smoothed histogram of the cue-presentations (pink) and touches of the target handle (gray) durations w.r.t. the movement onsets, i.e. releases of the starting handle. **B:** Classification accuracy for the range classifier using a window of 6 time points (blue) with the 95% confidence interval (shaded area) and the estimated chance level (grey). Lime bars indicate significant differences from the group level accuracy compared to the chance level (one-sided one-sample permutation t-test with 10,000 repetitions, $p_{crit} = 0.05$). **C:** Confusion matrix showing the predicted labels on the x-axis and the true labels on the y-axis for the peak accuracy of each subject between $t = 0$ s and $t = 1.5$ s. **D** and **E**, as in **B** and **C** but for single time point classification.

to chance level around the cue presentation and a smaller increase after the target cue presentation but with no significant differences (3.6 **B**). The accuracy evolution for the single time point approach is shown in Fig. 3.6 **E** and is similar to the windowed approach but with overall smaller accuracies and a shorter significant span from $t = -1.6$ s to $t = -1.5$ s and at $t = -1.2$ s (lime bars, one-sided one-sample permutation t-tests, $n=10,000$, $p_{crit} = 0.05$). Due to the two peaks, the confusion matrices for this classifier

were calculated once before the target cue presentation (Fig. 3.6 **C,F**) and once after the target cue presentation (Fig. 3.6 **D,G**). The average confusion matrices for the windowed approach reveal sustained correct predictions for right movements ($15.2\% \pm 2.8\%$ (mean \pm SD)) and left movements ($14.6\% \pm 2.2\%$ (mean \pm SD)), but the classifier seems to be more likely to confuse up and down movements with $12.9\% \pm 1.5\%$ (mean \pm SD) of true up movements being predicted as down movements while only $7.1\% \pm 2.0\%$ (mean \pm SD) of the predicted up movements were true up movements and vice versa for down movements with $12.3\% \pm 1.6\%$ (mean \pm SD) of true down movements being predicted as up movements and only $5.5\% \pm 1.6\%$ (mean \pm SD) of the predicted down movements were true down movements (Fig. 3.6 **C**). The same holds for the second confusion matrix, with overall lower true positives (Fig. 3.6 **C**). A similar pattern could be observed for the confusion matrices of the peak accuracies for the single time point approach before (Fig. 3.6 **F**) and after the movement (Fig. 3.6 **G**).

The direction classifier using only near trials and the cue-aligned epoching is shown in Fig. 3.7 with the smoothed movement on- and offsets in subfigure **A**. The accuracy evolution for the windowed approach shows an accuracy peak of 0.51 prior to the target cue presentation at $t = 0.7\text{s}$, declines to the estimated chance level (0.326) and stays slightly below the chance level until the end of the trial (3.7 **B**). Significant differences from chance level could be found from $t = -1.5\text{s}$ to $t = -0.6\text{s}$ and from $t = -0.4\text{s}$ to $t = -0.3\text{s}$ (lime bars, one-sided one-sample permutation t-tests, $n=10,000$, $p_{crit} = 0.05$). The corresponding average confusion matrices for the peak accuracy, once before the target cue presentation (3.7, **C**) and once after the target cue presentation (3.7, **D**) show no bias towards a class and no major confusions between classes, but clearly stronger true positive accuracies for the early time span ranging from $12.3\% \pm 2.9\%$ (mean \pm SD) to $14.2\% \pm 3.3\%$ (mean \pm SD) (, Fig. 3.7, **D**, main diagonal), while the true positive accuracies for the later time span range from $8.8\% \pm 2.0\%$ (mean \pm SD) to $10.2\% \pm 2.5\%$ (mean \pm SD) (Fig. 3.7, **D**, main diagonal). The accuracy evolution and the confusion matrices for the single time point approach are shown in Fig. 3.7 **E** and Fig. 3.7 **F**, **G**, respectively. The accuracy evolution shows a small peak of 0.39

3 Results

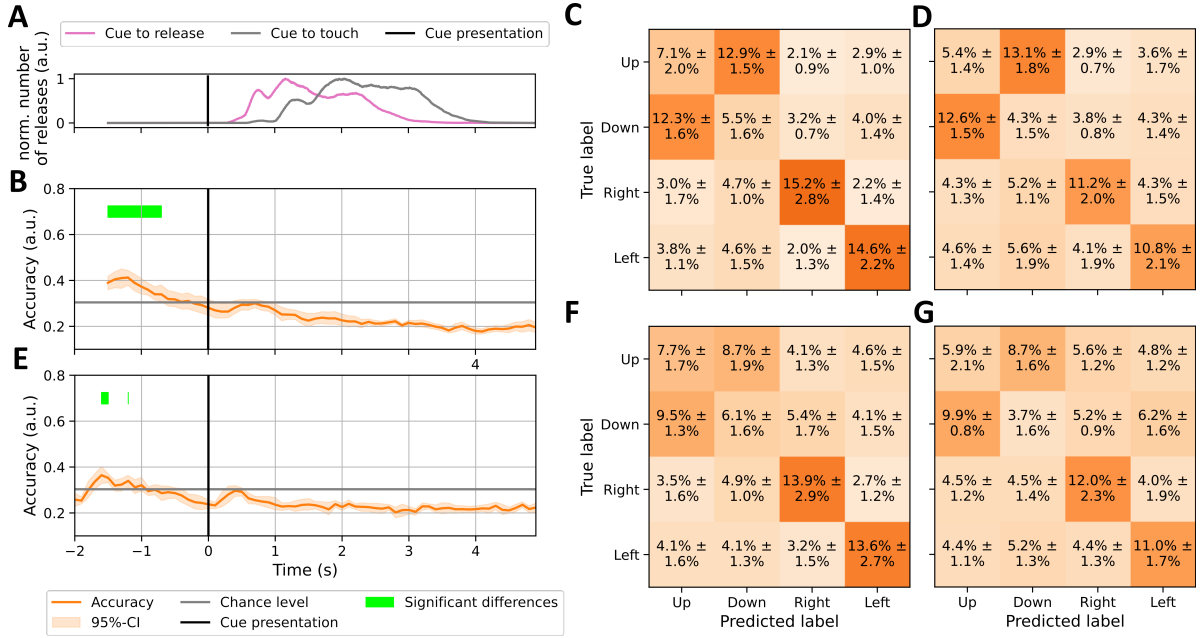


Figure 3.6: Direction classification cue-aligned. **A**: Smoothed histogram of the release (pink) and touch (gray) durations w.r.t. the cue presentation. **B**: Classification accuracy for the direction classifier using a window of 6 time points (orange) with the 95% confidence interval (shaded area) and the estimated chance level (grey). Lime bars indicate significant differences from the group level accuracy compared to the chance level (one-sided one-sample permutation t-test with 10,000 repetitions, $p_{crit} = 0.05$). **C**: Average confusion matrix showing the predicted labels on the x-axis and the true labels on the y-axis for the peak accuracy of each subject between $t = -2$ s and $t = -0.5$ s. **D**: Average confusion matrix showing the predicted labels on the x-axis and the true labels on the y-axis for the peak accuracy of each subject between $t = 0$ s and $t = 1.5$ s. **E**, **F** and **G**, as in **B**, **C** and **D** but for single time point classification.

at $t = 0.3$ s and a significant time window compared to chance level could be found from $t = -1.7$ – -1.5 (lime bars, one-sided one-sample permutation t-tests, $n=10,000$, $p_{crit} = 0.05$). The confusion matrix for the period prior to the target cue presentation shows no bias towards a class and its true positive accuracy range from $10.3\% \pm 2.6\%$ (mean \pm SD) to $12.5\% \pm 2.5\%$ (mean \pm SD) (Fig. 3.7 F, main diagonal). For the period after cue presentation, the accuracies are lower, ranging from $7.9\% \pm 2.2\%$ (mean \pm SD) to $9.5\% \pm 3.1\%$ (mean \pm SD) showing no bias towards a class.

Figure 3.8 shows the classification results for the direction classifier using only far trials

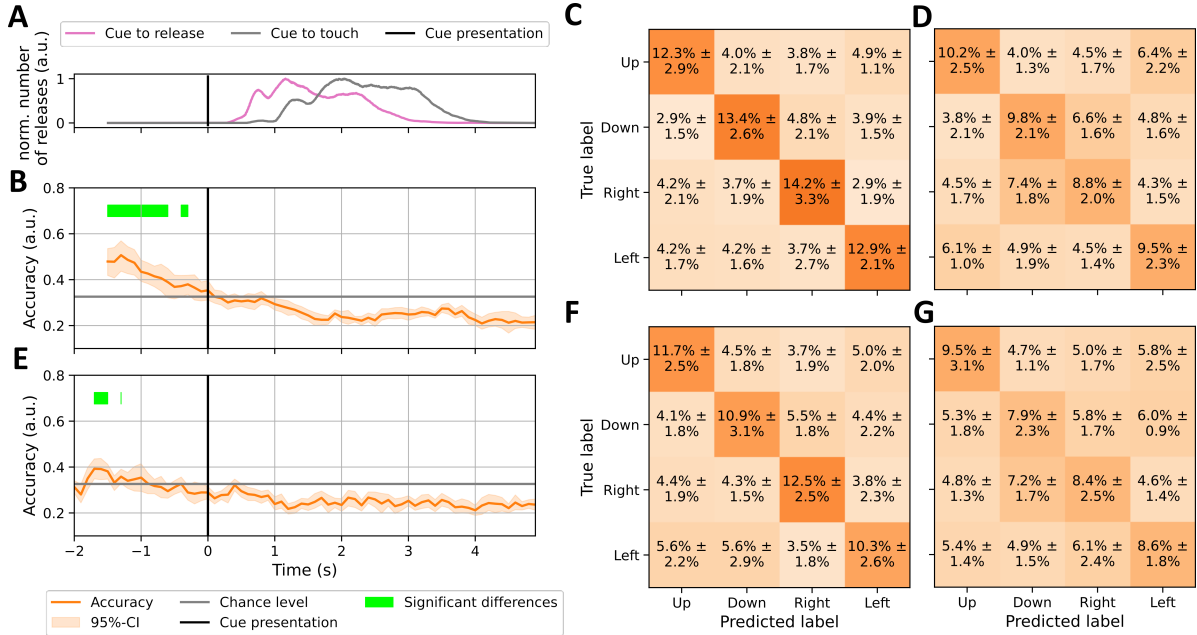


Figure 3.7: Near direction classification cue-aligned. **A:** Smoothed histogram of the release (pink) and touch (gray) durations w.r.t. the cue presentation. **B:** Classification accuracy for the near direction classifier using a window of 6 time points (orange) with the 95% confidence interval (shaded area) and the estimated chance level (grey). Lime bars indicate significant differences from the group level accuracy compared to the chance level (one-sided one-sample permutation t-test with 10,000 repetitions, $p_{crit} = 0.05$). **C:** Average confusion matrix showing the predicted labels on the x-axis and the true labels on the y-axis for the peak accuracy of each subject between $t = -2$ s and $t = -0.5$ s. **D:** Average confusion matrix showing the predicted labels on the x-axis and the true labels on the y-axis for the peak accuracy of each subject between $t = 0$ s and $t = 1.5$ s. **E, F** and **G**, as in **B, C** and **D** but for single time point classification.

for the cue-aligned approach. The smoothed histograms of the movements w.r.t. the target cue presentation are shown in Fig. 3.8, **A**. The classification accuracy development for the 6 time point (windowed) approach shows a first peak prior to the cue presentation of 0.48 at $t = -1.2$ s and remains significantly different from the estimated chance level (0.323) from $t = -1.5$ s to $t = -0.2$ s (lime bars, one-sided one-sample permutation t-tests, $n=10,000$, $p_{crit} = 0.05$) and a second peak can be seen after the target cue presentation of 0.44 at $t = 2.8$ s and being significantly different from chance level from $t = 0.3$ s to $t = 1.0$ s (lime bars, one-sided one-sample permutation t-tests, $n=10,000$,

$p_{crit} = 0.05$) (Fig. 3.8 **B**). The average confusion matrices for the windowed approach show no bias towards one class as well as no noticeably high miss classifications (Fig. 3.8 **C, D**). The true positive accuracies for the peak accuracies prior to the target cue presentation range from $11.8\% \pm 1.8\%$ (mean \pm SD) to $13.4\% \pm 2.3\%$ (mean \pm SD) (Fig. 3.8 **C**, main diagonal). For the peak accuracies after the target cue presentation, the true positive accuracies range from $10.9\% \pm 2.3\%$ (mean \pm SD) to $12.6\% \pm 3.5\%$ (mean \pm SD) (Fig. 3.8 **F**, main diagonal). The single time point classification accuracies show, similar to the windowed approach, two peaks but with shorter duration (Fig. 3.8 **E**). The first peak maxing at 0.41 can be found at $t = -1.6$ s being significantly different from chance level (0.323) from $t = -1.6$ s to $t = -1.5$ s (lime bars, one-sided one-sample permutation t-tests, $n=10,000$, $p_{crit} = 0.05$) and the second peak has a maximum of 0.38 at $t = 2.4$ s being significantly different from chance level from $t = 0.4$ s to $t = 0.5$ s (lime bars, one-sided one-sample permutation t-tests, $n=10,000$, $p_{crit} = 0.05$). The average confusion matrices of the peak accuracies for the first time span classifies right movements best with $13.0\% \pm 2.0\%$ (mean \pm SD) and the other 3 classes range from $9.9\% \pm 2.9\%$ (mean \pm SD) to $10.7\% \pm 1.6\%$ (mean \pm SD) (Fig. 3.8, **F**). The confusion matrix for the second peak shows no bias towards a class and ranges from $9.1\% \pm 2.4\%$ (mean \pm SD) to $11.5\% \pm 2.0\%$ (mean \pm SD) (Fig. 3.8, **G**).

3.2.2.2 Movement-aligned

Figure 3.9 shows the classification results for the direction classifier, using near and far trials, for the movement-aligned approach. The smoothed histogram of the target cue presentation (pink) and the duration until the target of the target handle (grey) are presented in Fig. 3.9 **A**. The evolution of the accuracy for the 6-point classifier starts to rise from below chance level, which was estimated to be 0.304 for this classifier, before the movement onset at $t = -0.1$ s to a peak of 0.46 at $t = 0.5$ s, after it declines to below chance level again (Fig. 3.9 **B**). Significant differences from chance level could be found from $t = 0.1$ s to $t = 1.2$ s (lime bars, one-sided one-sample permutation t-tests, $n=10,000$, $p_{crit} = 0.05$). The average confusion matrix for the peak subject accuracies

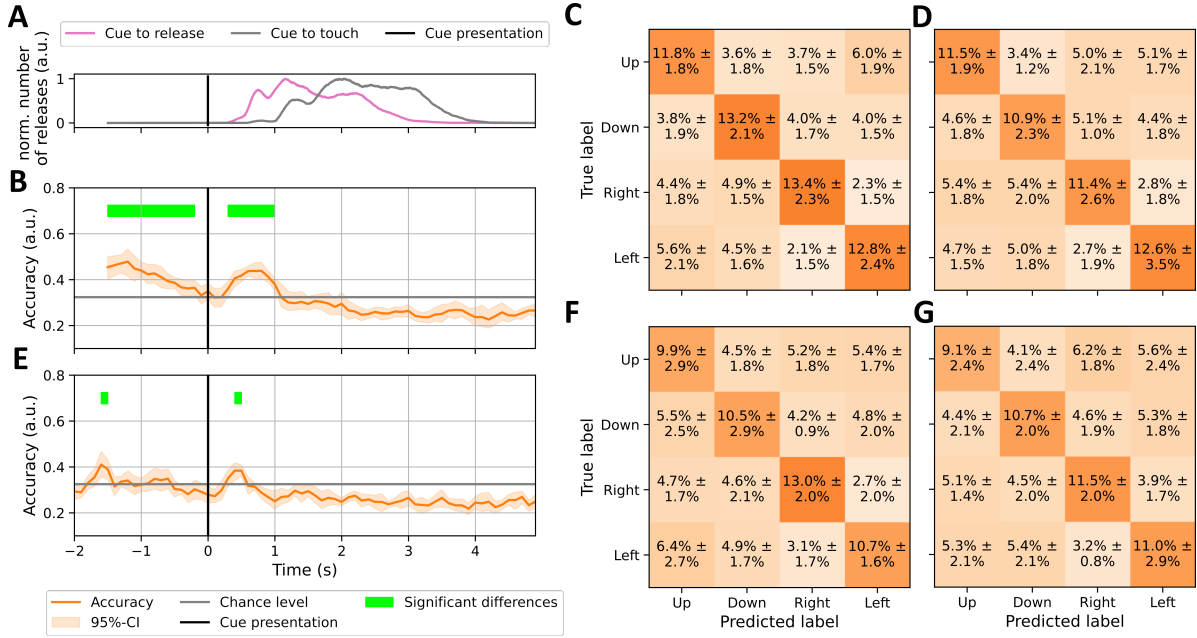


Figure 3.8: Far direction classification cue-aligned. **A:** Smoothed histogram of the release (pink) and touch (gray) durations w.r.t. the cue presentation. **B:** Classification accuracy for the far direction classifier using a window of 6 time points (orange) with the 95% confidence interval (shaded area) and the estimated chance level (grey). Lime bars indicate significant differences from the group level accuracy compared to the chance level (one-sided one-sample permutation t-test with 10,000 repetitions, $p_{crit} = 0.05$). **C:** Average confusion matrix showing the predicted labels on the x-axis and the true labels on the y-axis for the peak accuracy of each subject between $t = -2$ s and $t = -0.5$ s. **D:** Average confusion matrix showing the predicted labels on the x-axis and the true labels on the y-axis for the peak accuracy of each subject between $t = 0$ s and $t = 1.5$ s. **E, F** and **G**, as in **B, C** and **D** but for single time point classification.

shows, similar to the cue-aligned classifier, that up and down movements are more likely to be confused, while the classification for right and left movements is stable with true positive accuracies of $16.4\% \pm 3.0\%$ (mean \pm SD) $16.0\% \pm 3.6\%$ (mean \pm SD), respectively (Fig. 3.9 C). For the single time point classifier, the accuracy starts to rise at $t = -0.3$ s and rises to a peak of 0.43 at $t = 0.2$ s, finding a significant time span from $t = 0.0$ s to $t = 0.6$ s (lime bars, one-sided one-sample permutation t-tests, $n=10,000$, $p_{crit} = 0.05$) (Fig. 3.9 D). The same as for the windowed approach confusion matrix holds true for the single time point confusion matrix, where $13.9\% \pm 3.7\%$ (mean \pm SD)

of right movements and $12.9\% \pm 2.3\%$ (mean \pm SD) of left movements are classified correctly, but the classifier seems to confuse up and down movements (Fig. 3.9 E).

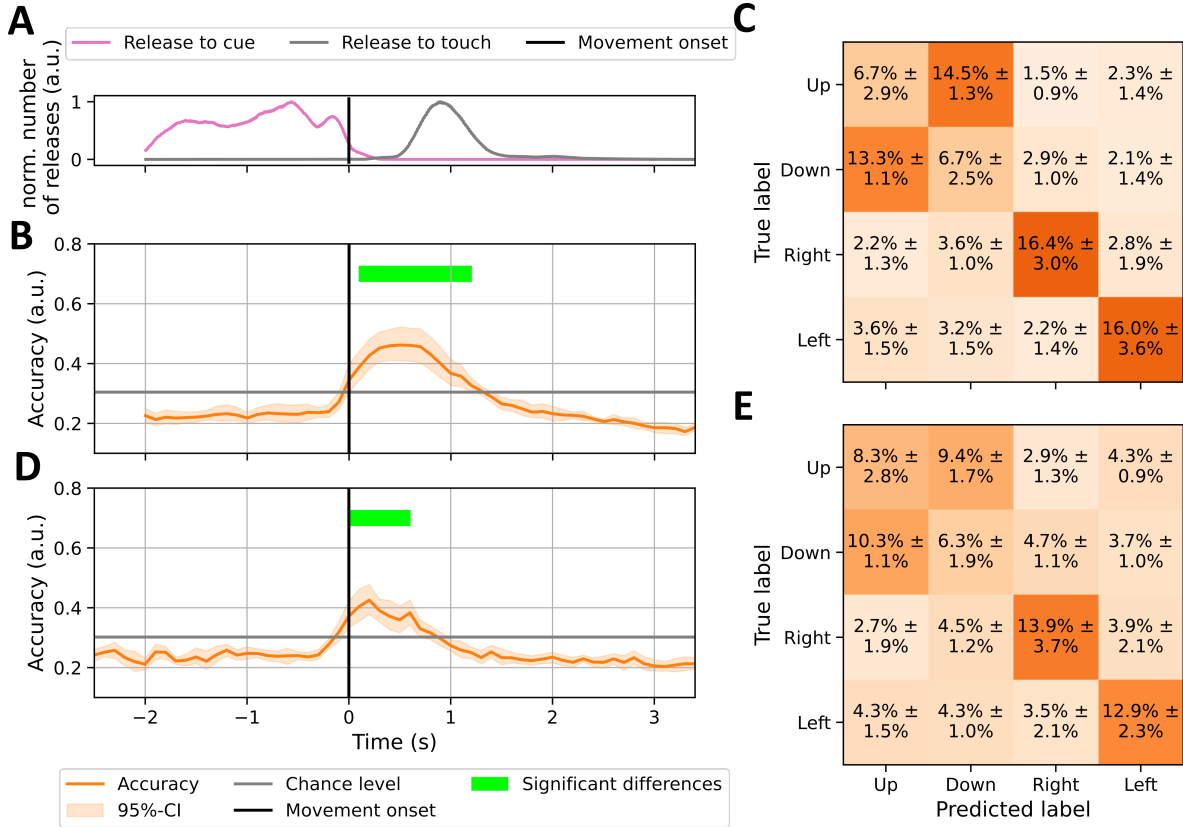


Figure 3.9: Direction classification movement-aligned. **A:** Smoothed histogram of the cue-presentations (pink) and touches of the target handle (gray) durations w.r.t. the movement onsets, i.e., releases of the starting handle. **B:** Classification accuracy for the direction classifier using a window of 6 time points (orange) with the 95% confidence interval (shaded area) and the estimated chance level (grey). Lime bars indicate significant differences from the group level accuracy compared to the chance level (one-sided one-sample permutation t-test with 10,000 repetitions, $p_{crit} = 0.05$). **C:** Confusion matrix showing the predicted labels on the x-axis and the true labels on the y-axis for the peak accuracy of each subject between $t = 0$ s and $t = 1.5$ s. **D** and **E**, as in **B** and **C** but for single time point classification.

The near direction classifier for movement-aligned epochs is depicted in Fig. 3.10. Again, the smoothed histogram of the target cue presentation (pink) and the duration until the touch of the target handle (gray) w.r.t. the release of the starting handle are presented in Fig. 3.10 A. The accuracy development for the windowed classifier

shows an increase from chance level (0.325) at $t = -0.2$ s, reaches a maximum of 0.55 at $t = 0.5$ s and reaches chance level again at $t = 0.3$ s, during the time window $t = 0.2$ s to $t = 1.2$ s, the accuracies are significantly different from chance level (lime bars, one-sided one-sample permutation t-tests, $n=10,000$, $p_{crit} = 0.05$) (Fig. 3.10 **B**). The average confusion matrix for the peak accuracies of all subjects show no bias towards a class and true positive accuracies range from $13.4\% \pm 5.1\%$ (mean \pm SD) to $14.5\% \pm 3.3\%$ (mean \pm SD) (Fig. 3.10 **C**, main diagonal). The single time point classifier shows a similar behaviour rising from chance level (0.325) at $t = -0.2$ s, reaching a maximum accuracy of 0.45 at $t = 0.2$ s and declining back to chance level at $t = 0.8$ s (Fig. 3.10 **D**). The average confusion matrix for peak accuracies shows no bias as well and true positive accuracies range from $11.0\% \pm 2.4\%$ (mean \pm SD) to $12.8\% \pm 4.4\%$ (mean \pm SD) (Fig. 3.10 **E**).

Figure 3.11 shows the classification results for the far direction classifier for the movement-aligned approach. The smoothed histogram of the target cue presentations (pink) and the durations until the touch of the target handle (grey) are presented in Fig. 3.11 **A**. The evolution of the accuracy for the 6-point classifier starts to rise from chance level (0.325) before the movement onset at $t = -0.1$ s to a peak of 0.62 at $t = 0.5$ s after it declines to below chance level again (Fig. 3.11 **B**). Significant differences from chance level could be found from $t = 0.0$ s to $t = 1.5$ s (lime bars, one-sided one-sample permutation t-tests, $n=10,000$, $p_{crit} = 0.05$). The average confusion matrix for the subjects peak accuracies reveals no bias towards a class and true positive accuracies range from $14.7\% \pm 3.6\%$ (mean \pm SD) to $16.8\% \pm 3.6\%$ (mean \pm SD) (Fig. 3.11 **C**). For the single time point classifier, the accuracy starts to rise at $t = -0.3$ s and reaches a peak of 0.52 at $t = 0.2$ s, finding a significant time span from $t = 0.0$ s to $t = 0.9$ s (lime bars, one-sided one-sample permutation t-tests, $n=10,000$, $p_{crit} = 0.05$) (Fig. 3.11 **D**). No bias towards a class could be found as well and the true positive accuracies are slightly lower, ranging from $13.1\% \pm 3.2\%$ (mean \pm SD) to $14.0\% \pm 4.3\%$ (mean \pm SD) (Fig. 3.11 **E**).

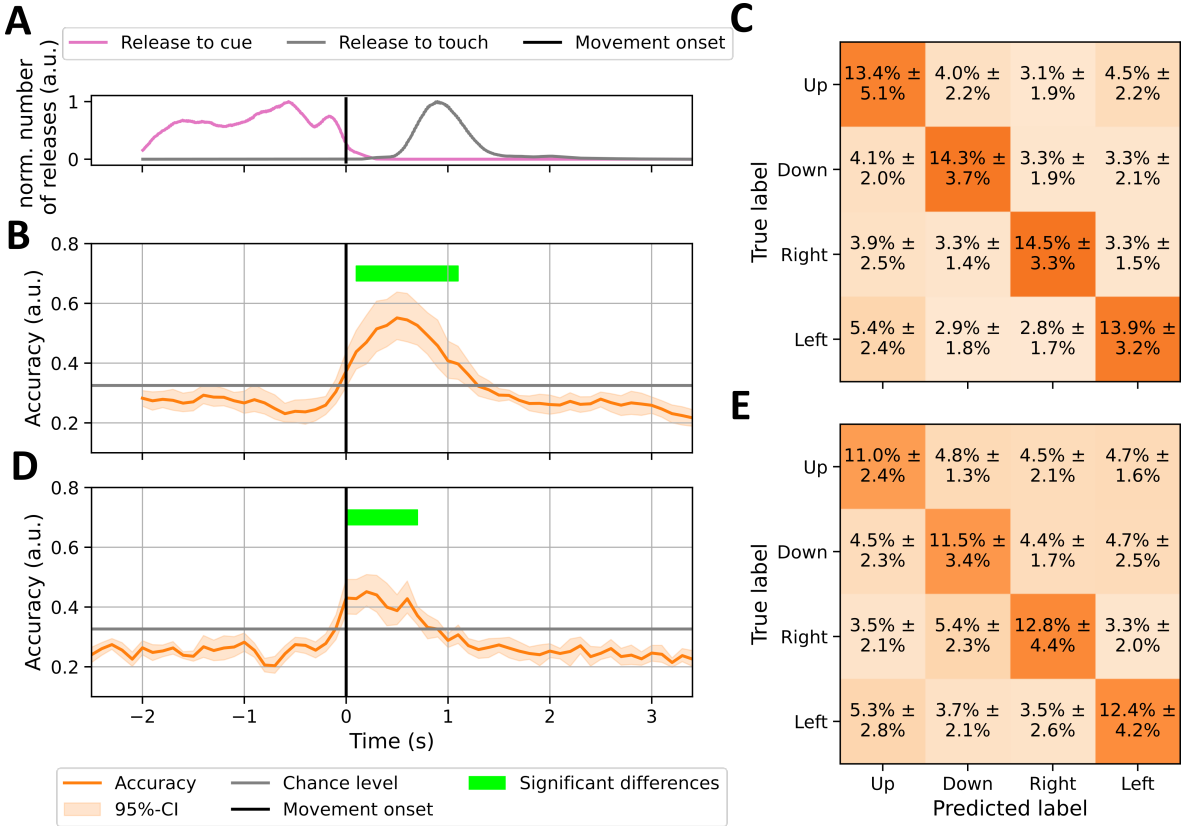


Figure 3.10: Near direction classification movement-aligned. **A:** Smoothed histogram of the cue-presentations (pink) and touches of the target handle (gray) durations w.r.t. the movement onsets, i.e., releases of the starting handle. **B:** Classification accuracy for the near direction classifier using a window of 6 time points (blue) with the 95% confidence interval (shaded area) and the estimated chance level (grey). Lime bars indicate significant differences from the group level accuracy compared to the chance level (one-sided one-sample permutation t-test with 10,000 repetitions, $p_{crit} = 0.05$). **C:** Confusion matrix showing the predicted labels on the x-axis and the true labels on the y-axis for the peak accuracy of each subject between $t = 0$ s and $t = 1.5$ s. **D** and **E**, as in **B** and **C** but for single time point classification.

3.2.3 Position classifier

3.2.3.1 Cue-aligned

The 5-class position sLDA classifier for the cue-aligned approach is shown in Fig. 3.12. The smoothed histograms of the movement durations w.r.t. the target cue presentation are depicted in Fig. 3.12 **A** for better visual alignment. The accuracy curve for the 6

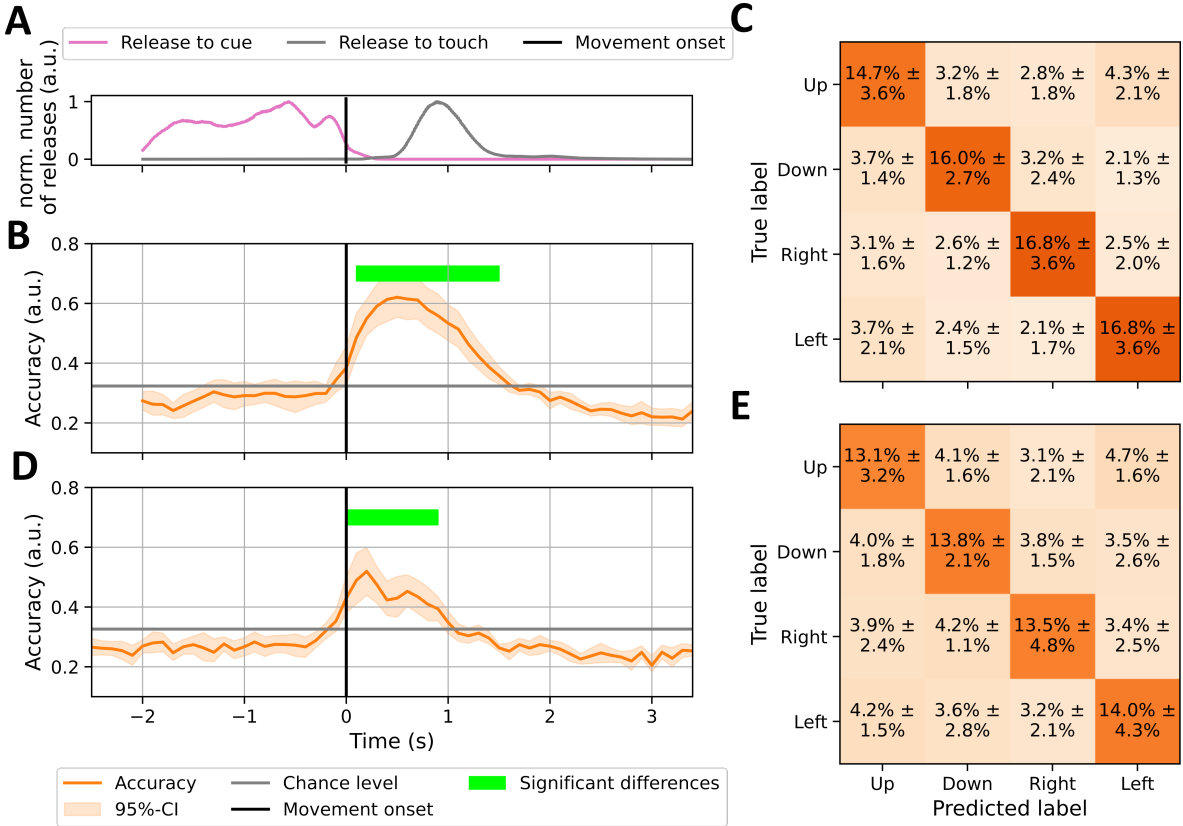


Figure 3.11: Far direction classification movement-aligned. **A:** Smoothed histogram of the cue-presentations (pink) and touches of the target handle (gray) durations w.r.t. the movement onsets, i.e., releases of the starting handle. **B:** Classification accuracy for the far direction classifier using a window of 6 time points (blue) with the 95% confidence interval (shaded area) and the estimated chance level (grey). Lime bars indicate significant differences from the group level accuracy compared to the chance level (one-sided one-sample permutation t-test with 10,000 repetitions, $p_{crit} = 0.05$). **C:** Confusion matrix showing the predicted labels on the x-axis and the true labels on the y-axis for the peak accuracy of each subject between $t = 0$ s and $t = 1.5$ s. **D** and **E**, as in **B** and **C** but for single time point classification.

time point classifier starts at a plateau slightly above chance level (0.262) prior to the target cue presentation and declines to chance level towards the target cue presentation at $t = 0$ s (Fig. 3.12 **B**). Right after the target cue presentation the accuracy rises at $t = 0.1$ s and reaches a maximum of 0.39 at $t = 0.7$ s before reaching chance level again at $t = 1.1$ s. Significant differences from chance level could be found from $t = -1.5$ s to $t = -0.6$ s, at $t = -0.2$ s and from $t = 0.3$ s to $t = 1.0$ s (lime bars, one-sided one-sample

permutation t-tests, $n=10,000$, $p_{crit} = 0.05$). The average confusion matrix of the peak subject accuracies for the time period prior to the target cue presentation shows that the 4 classes — top, bottom, right and left — are more likely to be correctly classified with true positive accuracies ranging from $6.9\% \pm 1.9\%$ (mean \pm SD) to $9.1\% \pm 2.5\%$ (mean \pm SD) but the center class cannot be distinguished from the others ($4.3\% \pm 1.2\%$ (mean \pm SD) true positive accuracy)(Fig. 3.12 **C**). For the period after the target cue presentation, the true positive accuracies for the classes top, bottom, right and left are similar to the first period, but the center class can be better distinguished with a true positive accuracy of $6.5\% \pm 2.1\%$ (mean \pm SD) (Fig. 3.12 **D**). The accuracy evolution for the single time point classifier fluctuates around chance level for the whole trial, with a small accuracy peak of 0.31 shortly after the target cue presentation at $t = 0.4$ s and a significant range from $t = 0.3$ s to $t = 0.5$ s (lime bars, one-sided one-sample permutation t-tests, $n=10,000$, $p_{crit} = 0.05$) (Fig. 3.12 **E**). The average confusion matrix for the period before the target cue presentation reveals that the bottom and right positions can be classified best ($7.7\% \pm 3.0\%$ (mean \pm SD) and $8.6\% \pm 2.1\%$ (mean \pm SD), respectively) (Fig. 3.12 **F**). For the period after the target cue presentation, no bias towards a class could be found, with true positive accuracies from $6.0\% \pm 3.0\%$ (mean \pm SD) to $7.0\% \pm 2.7\%$ (mean \pm SD) (Fig. 3.12 **G**).

3.2.3.2 Movement-aligned

The classification results for the movement-aligned approach are shown in Fig. 3.13. The smoothed histogram of the cue presentation timings and the grasps of the target handles w.r.t. to the release of the starting handle for better visual alignment are shown in Fig. 3.13 **A**. From the start of the trial, the accuracy curve for the 6 time point classifier fluctuates slightly below chance level (0.262) until $t = -0.2$ s and shows a bell-shaped curve until $t = 2$ s with a peak of 0.5 at $t = 0.7$ s and a range of time points where the accuracy is significantly different from chance level ranging from $t = 0.0$ s to $t = 1.6$ s (lime bars, one-sided one-sample permutation t-tests, $n=10,000$, $p_{crit} = 0.05$) (Fig. 3.13 **B**). The average confusion matrix of the subjects peak accuracies reveals

3 Results

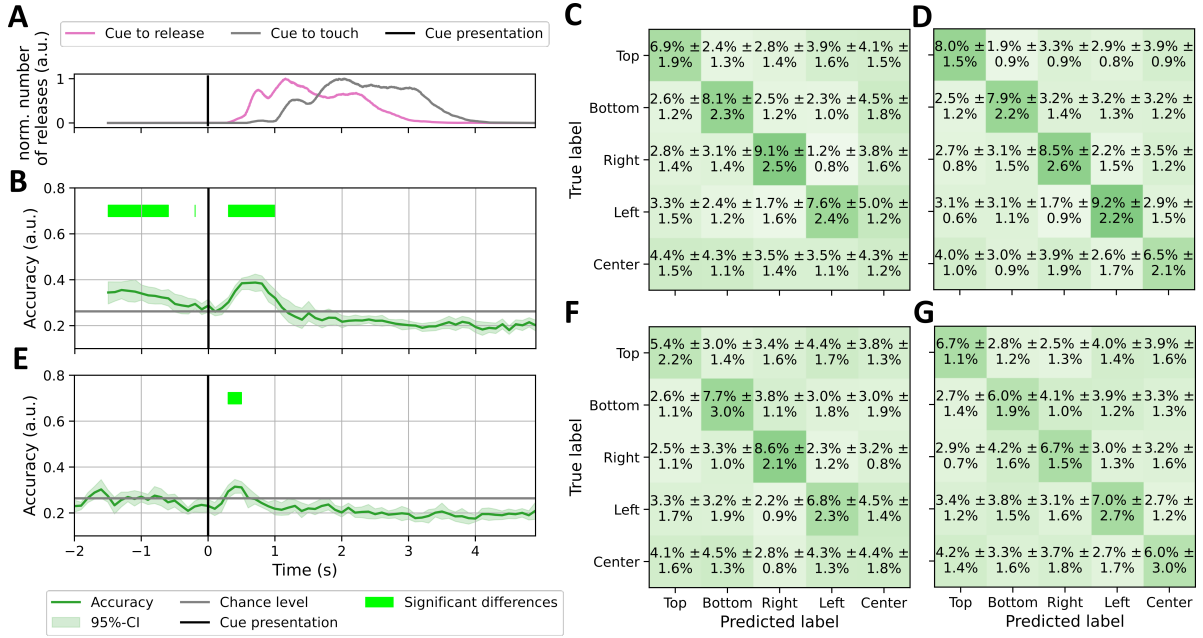


Figure 3.12: Position classification cue-aligned. **A:** Smoothed histogram of the release (pink) and touch (gray) durations w.r.t. the cue presentation. **B:** Classification accuracy for the position classifier using a window of 6 time points (green) with the 95% confidence interval (shaded area) and the estimated chance level (grey). Lime bars indicate significant differences from the group level accuracy compared to the chance level (one-sided one-sample permutation t-test with 10,000 repetitions, $p_{crit} = 0.05$). **C:** Average confusion matrix showing the predicted labels on the x-axis and the true labels on the y-axis for the peak accuracy of each subject between $t = -2$ s and $t = -0.5$ s. **D:** Average confusion matrix showing the predicted labels on the x-axis and the true labels on the y-axis for the peak accuracy of each subject between $t = 0$ s and $t = 1.5$ s. **E, F** and **G**, as in **B, C** and **D** but for single time point classification

that the center class is less likely to be predicted correctly with a true positive accuracy of $7\% \pm 4.1\%$ (mean \pm SD) compared to the other classes, where the true positive accuracies range from $10.1\% \pm 3.0\%$ (mean \pm SD) to $11.7\% \pm 2.8\%$ (mean \pm SD) (Fig. 3.13 **C**). Similar results but lower and shorter in accuracy and time can be seen for the single time point classifier, where the accuracy has a maximum of 0.4 at $t = 0.2$ s and a range of significantly higher accuracies than chance level from $t = 0.0$ s to $t = 1.0$ s (lime bars, one-sided one-sample permutation t-tests, $n=10,000$, $p_{crit} = 0.05$) (Fig. 3.13). The average confusion matrix shows that the classifier performs worst for the center class

($7.0\% \pm 3.8\%$ (mean \pm SD)) but the difference to the other classes is not as high as for the windowed approach, ranging from $9.0\% \pm 2.0\%$ (mean \pm SD) to $9.8\% \pm 3.9\%$ (mean \pm SD) (Fig. 3.13 E).

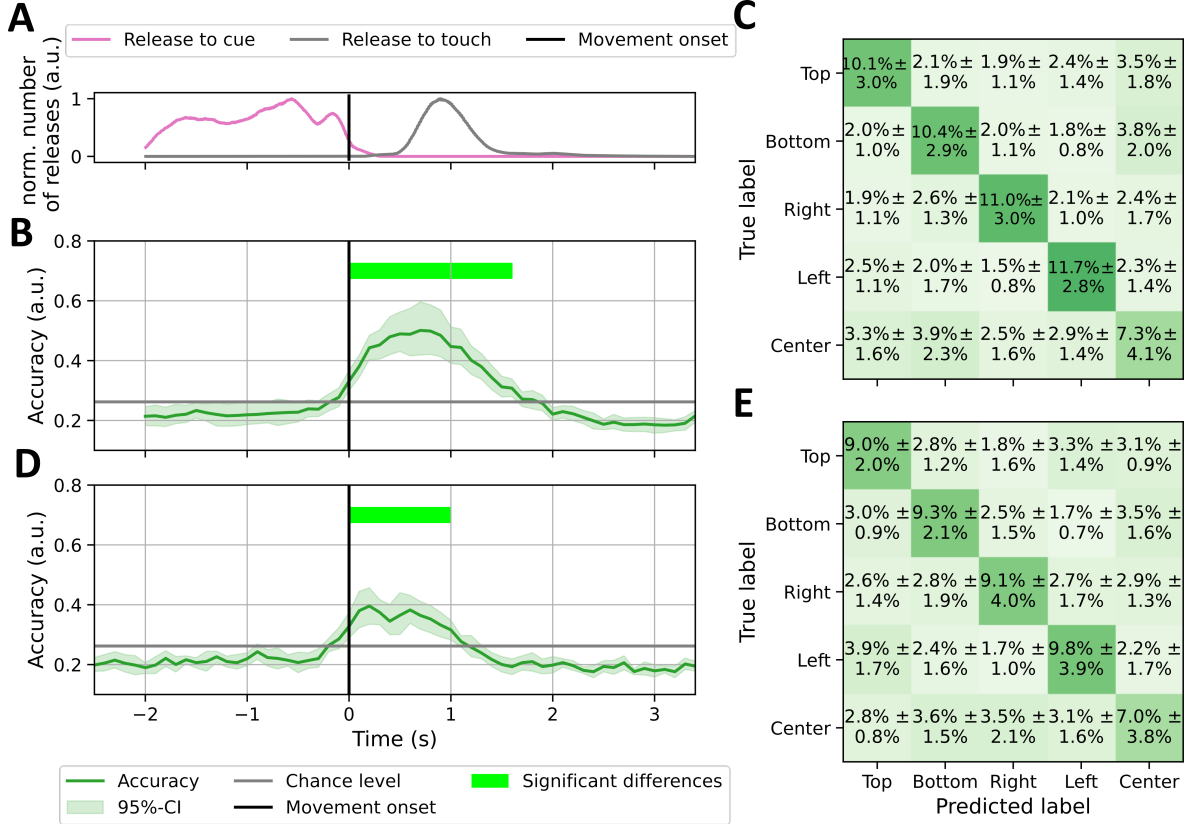


Figure 3.13: Position classification movement-aligned. **A:** Smoothed histogram of the cue-presentations (pink) and touches of the target handle (gray) durations w.r.t. the movement onsets, i.e. releases of the starting handle. **B:** Classification accuracy for the position classifier using a window of 6 time points (green) with the 95% confidence interval (shaded area) and the estimated chance level (grey). Lime bars indicate significant differences from the group level accuracy compared to the chance level (one-sided one-sample permutation t-test with 10,000 repetitions, $p_{crit} = 0.05$). **C:** Confusion matrix showing the predicted labels on the x-axis and the true labels on the y-axis for the peak accuracy of each subject between $t = 0$ s and $t = 1.5$ s. **D** and **E**, as in **B** and **C** but for single time point classification.

3.3 Encoding of range and direction

3.3.1 Cue-aligned

Figure 3.14 shows the results of the GLM for the cue-aligned approach evaluating each factor of the GLM, namely near, far, horizontal, vertical, and the intercept term. The factors encoding the range, i.e., near and far movements (Fig. 3.14 **A** and **B**), show similar responses as do the factors encoding direction, i.e., horizontal and vertical movements (Fig. 3.14 **C** and **D**). At the target cue presentation ($t = 0\text{ s}$) significant group level differences could be revealed for near (Fig. 3.14 **A**) and far (Fig. 3.14 **B**) movements in central and occipital regions and a parieto-occipital response contralateral to the executing limb, at $t = 0.1\text{ s}$. 400 ms after the presentation of the target cue, a response in the frontal areas again encodes the range parameter. From $t = 0.7\text{ s}$ to $t = 0.9\text{ s}$ regression parameters at fronto-central and parieto-occipital channels showed significant group level differences from 0 for the range conditions as well. Central and parieto-occipital channels encode the direction parameters around the target cue presentation at $t = 0.0\text{ s}$ to $t = 0.1\text{ s}$ for horizontal (Fig. 3.14 **C**) and vertical (Fig. 3.14 **D**) factors, from $t = 0.2\text{ s}$ to $t = 0.3\text{ s}$ the encoding of direction moves more frontal lateralized to the left hemisphere. For $t = 0.5\text{ s}$ to $t = 0.6\text{ s}$ left parietal channels and occipital channels showed significantly different regression factors. The intercept term (Fig. 3.14 **E**) shows significant regression coefficients at fronto-central channels as well as at parieto-occipital channels from $t = 0.2\text{ s}$ to $t = 0.4\text{ s}$ and a broad response over the whole head surface at $t = 0.8\text{ s}$ to $t = 0.9\text{ s}$. The factors encoding the intercept term reveal a fronto-central response from $t = 0.2\text{ s}$ to $t = 0.4\text{ s}$ and a temporal-occipital response at $t = 0.4\text{ s}$. At $t = 0.8\text{ s}$ to $t = 0.9\text{ s}$ central channels encode the intercept term, i.e., the grand average activity.

Figure 3.15 depicts the results of the comparison of encoded conditions. Differences in the regression coefficients for the range parameter, i.e., near vs. far movements, reveal differences in central and occipital channels around the target cue presentation ($t = 0.0\text{ s}$) and in mainly central channels from $t = 0.4\text{ s}$ to $t = 0.5\text{ s}$, from $t = 0.7\text{ s}$

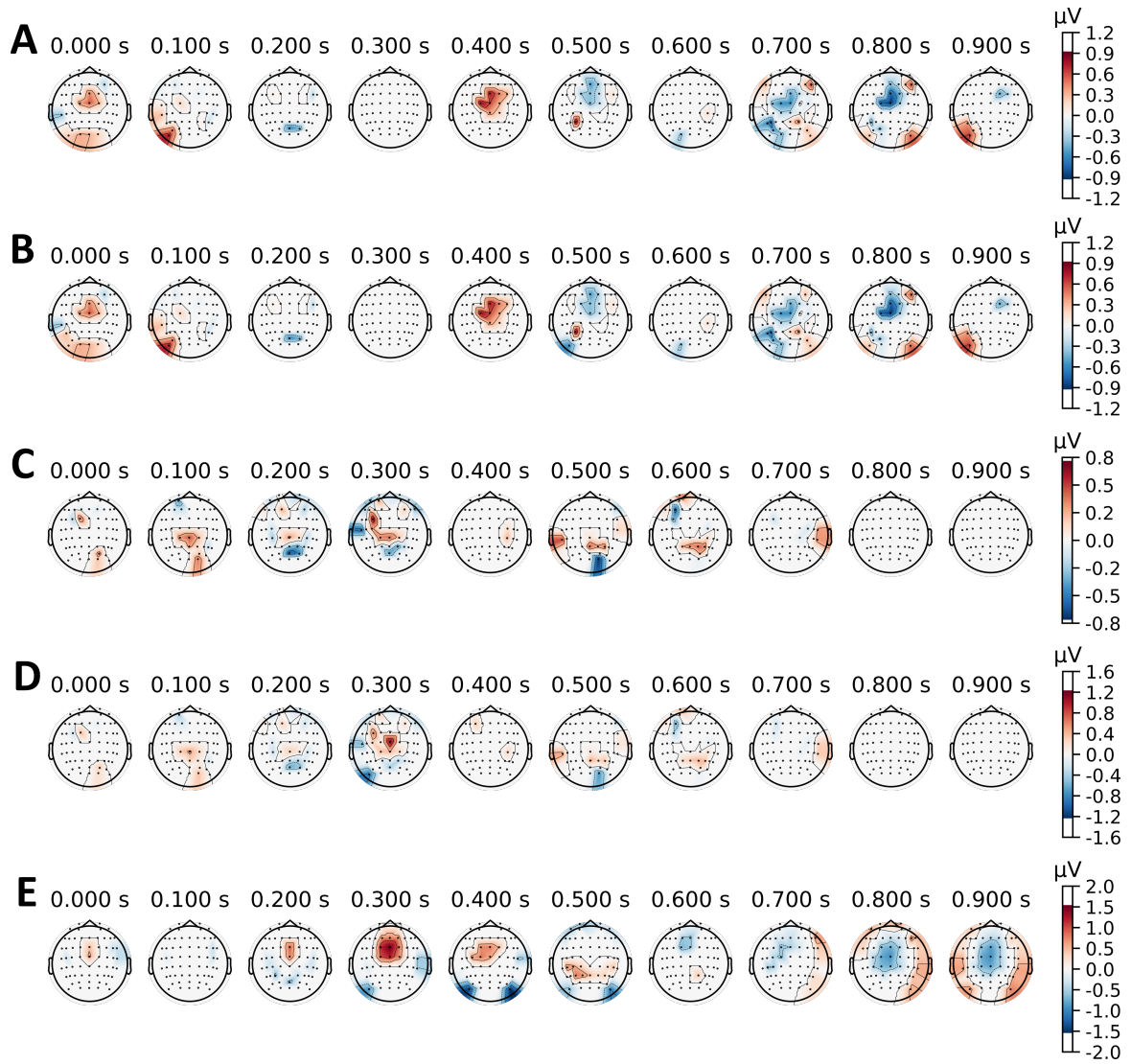


Figure 3.14: GLM results cue-aligned for the regression coefficients. Remapped EEG activity where the regression coefficients for the encoded conditions in the GLM are significantly different from 0 (two-sided one sample permutation t-tests with 10,000 permutations, $p_{crit} = 0.05$). **A** Near movements. **B** Far movements. **C** Horizontal movements. **D** Vertical movements. **E** Intercept term.

to $t = 0.8$ s differences could be found across the whole scalp (Fig. 3.15 **A**). For the direction parameter, differences could be found in central to occipital channels right after the target cue presentation and in central and occipital channels of the left hemisphere after 0.3 s (Fig. 3.15 **B**). The comparison of the range and direction parameters reveals differences in frontal and central channels from $t = 0.0$ s to $t = 0.2$ s and adding more

channels across the whole scalp from $t = 0.3\text{ s}$ to $t = 0.5\text{ s}$ (Fig. 3.15).

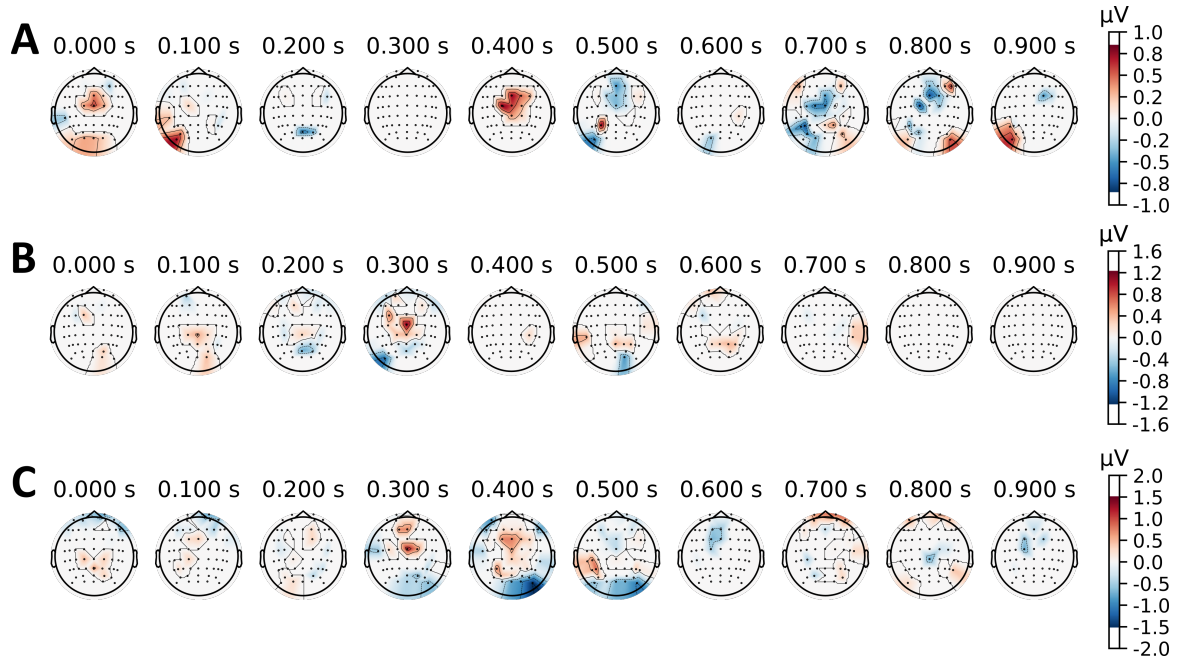


Figure 3.15: GLM results cue-aligned comparing the conditions. Comparison of encoded conditions in the form of remapped EEG activity for channels with significant group level differences of the regression coefficients (two-sample two-sided permutation t-tests, 10,000 permutations, $p_{crit} = 0.05$). **A** Near vs. far movements **B** Horizontal vs. vertical movements **C** Range vs. direction.

3.3.2 Movement-aligned

The results of the GLM for the movement-aligned approach are shown in Figure 3.16, evaluating each factor of the GLM (near, far, horizontal, vertical and the intercept term). Similar to the cue-aligned approach, the factors encoding the range, i.e., near and far movements (Fig. 3.16 **A** and **B**), show similar responses, as do the, factors encoding direction, i.e., horizontal and vertical movements (Fig. 3.16 **C** and **D**). 400 ms prior to the release of the starting handle, the frontal and occipital channels show significant differences from zero for the regression coefficients encoding near (Fig. 3.16 **A**) and far (Fig. 3.16 **B**) movements. At $t = 0.2\text{ s}$, a few parieto-occipital channels encode the range condition and at $t = 0.2\text{ s}$ a response in central channels could be found moving to fronto-

central channels towards the end at $t = 0.4$ s. The regression coefficients for horizontal (Fig. 3.16 **C**) and vertical (Fig. 3.16 **D**) movements are encoded around the movement onset from $t = -0.1$ s to $t = 0.0$ s in the fronto-central region and on the left hemisphere in the parieto-occipital region, as well as in frontal and central channels at $t = 0.2$ s and in central and occipital regions at $t = 0.3$ s. The intercept term, representing the grand average activity of all trials, is encoded in frontal regions from 500 ms to 400 ms before the movement onset and all over the scalp from $t = -0.2$ s to $t = -0.1$ s, after the movement onset in frontal and central channels ($t = 0.1$ s) fading to only central regions towards $t = 0.4$ s.

Figure 3.17 shows the results of the comparison of encoded conditions for the movement-aligned approach. The results for the range parameter are shown in Fig. 3.17 **B** and reveal the most channels with differences located in frontal and occipital channels at $t = -0.4$ s and only in a few channels in the frontal and central regions from $t = -0.2$ s to $t = 0.4$ s. For the direction parameter, differences were found in frontal and central regions at $t = -0.3$ s and $t = -0.2$ s, in frontal and left-sided parieto-occipital channels at $t = -0.1$ s and $t = 0.0$ s and in fronto-central and occipital channels from $t = 0.2$ s to $t = 0.3$ s. Differences between factors encoding range and factors encoding direction could be observed in central and frontal channels from $t = -0.1$ s until $t = 0.4$ s (Fig. 3.17 **C**).

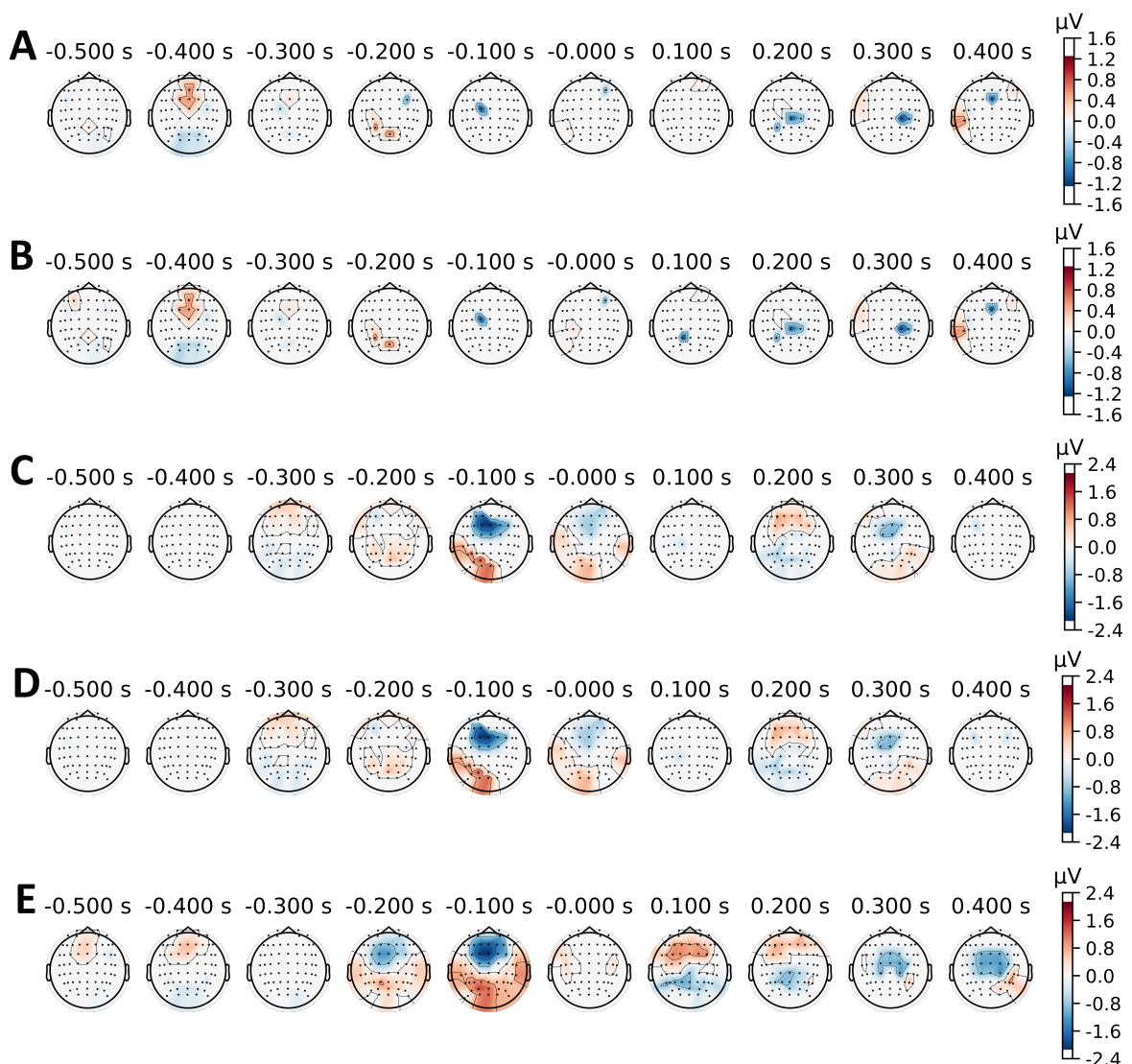


Figure 3.16: GLM results movement-aligned for the regression coefficients. Remapped EEG activity where the regression coefficients for the encoded conditions in the GLM are significantly different from 0 (two-sided one sample permutation t-tests with 10,000 permutations, $p_{crit} = 0.05$). **A** Near movements. **B** Far movements. **C** Horizontal movements. **D** Vertical movements. **E** Intercept term.

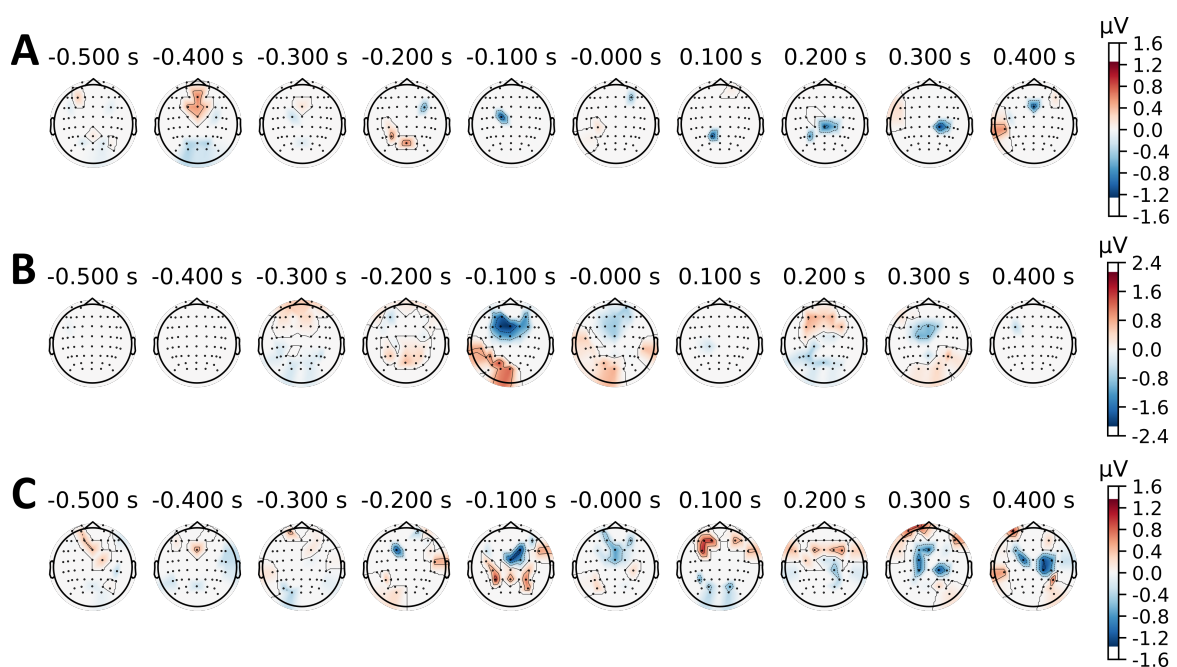


Figure 3.17: GLM results movement-aligned comparing the conditions. Comparison of encoded conditions in the form of remapped EEG activity for channels with significant group level differences of the regression coefficients (two-sample two-sided permutation t-tests, 10,000 permutations, $p_{crit} = 0.05$). **A** Near vs. far movements **B** Horizontal vs. vertical movements **C** Range vs. direction.

4 Discussion

This chapter focuses on the critical interpretation of the results in relation to the methods used and in the context of other research findings.

4.1 Temporal results

First, it was investigated whether the observed movements were indeed self-paced movements from the participants, in order to be able to investigate the different neural responses associated with movement preparation (cue-aligned) and movement initiation and execution (movement-aligned). The findings of Figure 3.1 suggest that this holds true in general, as the average time between target cue presentation and release of the target handle was at 1.41 s and 1.38 s for near and far movements, respectively and no significant differences were found between the conditions. However, looking at the smoothed histogram of the movement onsets (e.g., at Fig. 3.2, **A** top) one can see that the movement onset distribution has one smaller early peak immediately after the target cue presentation, followed by a bigger second peak at approximately $t = 1$ s. This first peak can be attributed to subject A01, which released the target handle immediately after the target cue presentation, most likely due to poor instruction.

The grand average responses for the cue-aligned approach are in line with results from Kobler et al. [22] showing a VEP after target cue presentation followed by a negative deflection after around 800 ms at fronto-central channels. Significant differences after the target cue presentation between far and near trials at the selected channels may

already indicate the distinguishability of different ranges.

The movement aligned temporal results revealed a MRCP with a steep negative deflection, which can be attributed to the Bereitschaftspotential, followed by an oscillation with a time constant of around half a second. This oscillation may be ascribed to the complexity of the movement, as the movement starts with opening the hand, i.e., releasing a palmar grasp, before reaching to the target handle. Schwarz et al. have observed similar MRCP shapes investigating different grasp types [41]. Significant differences between far and near trials after around 1.3 s can be attributed to the longer reach movements for far trials.

During the movement-aligned approach, movement-related artifacts of the neck and shoulder muscles could have contaminated the EEG. As no lateralized activity at temporal channels could be found (Fig. 3.3, C) and by applying strict epoch exclusion criteria (visually and based on amplitude) it can be surmised that any residual movement artifacts reflected in the EEG did not interfere with nor bias the classifications.

4.2 Classification analysis

The overall classification results showed that both classification approaches, windowed and single time point, provided comparable results. As expected, the classifier that uses 6 time points as features provides more sustainable results than the classifier that uses one time point, making the windowed classifier very suitable for offline analysis. However, since 5 previous time points and the current time point are required, this classifier may not be very well suited for online BCI applications where rapid feedback is preferred during training for improving BCI systems [42].

The range classifier revealed that it is possible to distinguish between different ranges during movement preparation right after the participant gets the information of the target position with accuracies of 64% (Fig. 3.4), as well as during the initiation and execution of the movement, where a longer period of a significant increase in accuracy could be observed achieving accuracies of 69% (Fig. 3.5. As the trials were split into

near and far movements, with all four starting positions evenly distributed across these two classes (near and far), it can be concluded that the range parameter is independent from directional processing. No bias towards one class was observed in the classification.

For the direction classifiers, similar accuracies in the cue-aligned approach could be observed prior to the target cue presentation regardless of the subcondition, i.e., direction (Fig. 3.6), near direction (Fig. 3.7), far direction (Fig. 3.8), but very different accuracy curves after the target cue presentation were revealed. This similarities and differences can be explained by the paradigm. At the beginning of a trial, the participants received the visual cue for the starting handle, which was always one of the 4 outer handles, and immediately reached for it. Therefore, the classifier distinguishes between these 4 conditions, which are a combination of movement preparation and execution. After the cue presentation, the far direction classifier shows the best performance, the direction classifier, containing near and far trials, performs worse with no significant differences from chance level but an observable increase after the target cue presentation and the near direction classifier performs worst after the target cue presentation. When looking at the paradigm again, for the far direction classifier, only one of the outer handles could be one of the target handles which leaves 4 different handles as the target handle and 4 directions that can be distinguished by a 4 class classifier, but it cannot be told whether the directions or the positions are the classes that are separated. For the near direction classifier, the target handle would always be the center target which leaves only one handle as the target handle and as no increase in accuracy can be seen for the classifier that aims to separate 4 classes as there are 4 directions it could be that there is truly only one class encoded during movement planning, namely the center position. For the combined classifier, the 4 outer handles and the center handle are possible target handles, leaving 5 possible handles. Therefore, it could be that the 4-class classifier cannot distinguish between the 5 handles. This means that the results suggest that instead of encoding directions, which were 4 in all classifiers, during movement preparation, it seems more likely that the brain encodes positions. This findings are

further investigated in the position classifier.

The accuracy curves of the position classifier (Fig. 3.12, **B** and **E**) for the cue-aligned approach show a significant increase in accuracy after the target cue presentation, which supports the previous findings from the direction classifier, that the brain encodes positions instead of directions during movement preparation. The average confusion matrices for the time period prior to the target cue-presentation (Fig. 3.12 **C** and **F**), where only 4 classes were possible (top, bottom, right, left), reveal that indeed only those 4 classes were likely to be classified. Looking at the confusion matrices after the target cue presentation (Fig. 3.12 **D** and **G**), where 5 classes were possible (top, bottom, right, left, center), all 5 classes were likely to be classified correctly, but with the center class being predicted correctly slightly less than the other classes. This leads to the assumption that the brain may mainly encode positions as features during directional movement preparation instead of directions.

For all classifiers, the movement-aligned approach delivered better results in peak accuracies and longer durations of sustained accuracies above the chance level.

4.3 Encoding of range and direction

For the cue-aligned setting, channels related to direction were found earlier (0.3 s after cue presentation) than channels related to range (0.4 s after cue presentation) (Fig. 3.14). This is in line with the classification results, where the significant period for the direction/position classifier starts at 0.3 s and the significant period for the range classifier starts at 0.4 s. The activity could be decoded in fronto-central channels, while channels encoding direction were more scattered.

The movement-aligned results revealed that frontal and parieto-occipital channels around 400 ms prior to movement onset may encode information about range, while fronto-central and contralateral temporal and occipital channels 100 ms before the movement onset encode information about direction (Fig. 3.16).

Differences between far vs. near and horizontal vs. vertical encoded channels were

found in the same regions as they were found for range and direction, for both approaches (Fig. 3.15 and Fig. 3.17) validating the assumption that there are distinct regions for the processing of different parameters like range or direction.

5 Conclusion

Prior work has studied the delta band activity of movement preparation and directional processing [22]. In this thesis, the involvement of a range parameter in the movement preparation and execution of self-paced voluntary upper limb movement was studied. Evidence that information about the range of a movement can be decoded from both the movement preparation (aligned to a target cue) and the movement initiation and execution (movement aligned) could be revealed. Additionally, it could be shown that this range parameter is independent of the direction, indicating that the range is represented as a relative parameter with respect to the current arm or hand position.

The extraction of range parameters prior to a movement (cue-aligned) could be useful for future BCI systems, e.g., to give state-of-the art movement decoders more confidence by extracting a possible movement distance before the start of a movement.

One limitation of the work was the presence of only two ranges, i.e., wide and narrow movements. One possibility for future work is to investigate how finely one can granulate different distances and still detect them as differences in the EEG.

In this study, the range parameter was investigated on a vertical board. This means the movement took place in x and z direction. While Pulferer et al. (2022) found preferences towards the x-coordinate during continuous 2D trajectory decoding on a horizontal plane (x-y-directions) [43], no preferences towards a coordinate could be observed in this study, leading to the assumption that it may be more difficult to extract depth information from EEG. However, to further investigate this claim a 3 dimensional approach could be used similar to Collinger et al. (2013) [17].

The direction and position classifiers revealed that the position of a target held more

information than the direction in which a movement was executed. These findings may suggest that discrete targets are encoded in a system of coordinates rather than in directional vectors. One approach to further investigate this claim could be to use a one-dimensional center-out task, using at least 2 distances on either side of the center and then cross out the positions and directions in the analysis.

Another limitation could be the relatively high proportion of discarded trials of about 22 % where especially the classifiers using 4 or 5 classes have a low sample size.

The decoding of conditions revealed distinct regions encoding the range parameter in movement preparation, which is temporally aligned with the peak accuracy of the range classifier. These findings could be further extended to source space using source localization to get a more detailed insight into the involved regions.

Bibliography

- [1] J. Wolpaw and E. W. Wolpaw, *Brain–Computer Interfaces: Principles and Practice*. Oxford University Press, Jan. 2012.
- [2] M. A. Goodale, J. P. Meenan, H. H. Bülthoff, D. A. Nicolle, K. J. Murphy, and C. I. Racicot, “Separate neural pathways for the visual analysis of object shape in perception and prehension,” *Current Biology*, vol. 4, no. 7, pp. 604–610, 1994.
- [3] M. N. Hebart and G. Hesselmann, “What visual information is processed in the human dorsal stream?” *Journal of Neuroscience*, vol. 32, no. 24, pp. 8107–8109, 2012.
- [4] M. Jahanshahi, G. Dirnberger, A. Liasis, A. Towell, and S. Boyd, “Does the prefrontal cortex contribute to movement-related potentials? Recordings from subdural electrodes,” *Neurocase*, vol. 7, no. 6, pp. 495–501, 2001.
- [5] G. Mihailoff and D. Haines, “Motor system II: corticofugal systems and the control of movement,” *Fundamental Neuroscience*. New York, NY: Churchill Livingstone Inc, pp. 335–346, 1997.
- [6] S. Kakei, D. S. Hoffman, and P. L. Strick, “Muscle and movement representations in the primary motor cortex,” *Science*, vol. 285, no. 5436, pp. 2136–2139, 1999.
- [7] C. Henley, *Foundations of Neuroscience*. Michigan State University Libraries, 2021, ISBN: 978-1-62610-109-8.

- [8] G. R. Müller-Putz, R. J. Kobler, J. Pereira, *et al.*, “Feel your reach: An EEG-based framework to continuously detect goal-directed movements and error processing to gate kinesthetic feedback informed artificial arm control,” *Frontiers in Human Neuroscience*, vol. 16, p. 841312, 2022.
- [9] M. Teplan *et al.*, “Fundamentals of EEG measurement,” *Measurement Science Review*, vol. 2, no. 2, pp. 1–11, 2002.
- [10] T. Kirschstein and R. Köhling, “What is the source of the EEG?” *Clinical EEG and Neuroscience*, vol. 40, no. 3, pp. 146–149, 2009.
- [11] G. Pfurtscheller, C. Neuper, G. Muller, *et al.*, “Graz-BCI: state of the art and clinical applications,” *IEEE Transactions on Neural Systems and Rehabilitation Engineering*, vol. 11, no. 2, pp. 1–4, 2003.
- [12] G. R. Müller-Putz, A. Schwarz, J. Pereira, and P. Ofner, “From classic motor imagery to complex movement intention decoding: the noninvasive Graz-BCI approach,” *Progress in Brain Research*, vol. 228, pp. 39–70, 2016.
- [13] M. Hallett, “Movement-related cortical potentials.,” *Electromyography and Clinical Neurophysiology*, vol. 34, no. 1, pp. 5–13, 1994.
- [14] H. Shibasaki and M. Hallett, “What is the Bereitschaftspotential?” *Clinical Neurophysiology*, vol. 117, no. 11, pp. 2341–2356, 2006.
- [15] H. H. Kornhuber and L. Deecke, “Hirnpotentialänderungen bei Willkürbewegungen und passiven Bewegungen des Menschen: Bereitschaftspotential und reafferente Potentiale,” *Pflüger’s Archiv für die gesamte Physiologie des Menschen und der Tiere*, vol. 284, pp. 1–17, 1965.
- [16] H. Shibasaki, G. Barrett, E. Halliday, and A. Halliday, “Components of the movement-related cortical potential and their scalp topography,” *Electroencephalography and Clinical Neurophysiology*, vol. 49, no. 3-4, pp. 213–226, 1980.
- [17] J. L. Collinger, B. Wodlinger, J. E. Downey, *et al.*, “High-performance neuroprosthetic control by an individual with tetraplegia,” *The Lancet*, vol. 381, no. 9866, pp. 557–564, 2013.

- [18] G. R. Müller-Putz, V. Mondini, V. Martinez-Cagigal, *et al.*, “Decoding of continuous movement attempt in 2-dimensions from non-invasive low frequency brain signals,” in *2021 10th International IEEE/EMBS Conference on Neural Engineering (NER)*, IEEE, 2021, pp. 322–325.
- [19] P. Ofner, A. Schwarz, J. Pereira, and G. R. Müller-Putz, “Upper limb movements can be decoded from the time-domain of low-frequency EEG,” *PLOS ONE*, vol. 12, no. 8, e0182578, 2017.
- [20] V. Mondini, R. J. Kobler, A. I. Sburlea, and G. R. Müller-Putz, “Continuous low-frequency EEG decoding of arm movement for closed-loop, natural control of a robotic arm,” *Journal of Neural Engineering*, vol. 17, no. 4, p. 046 031, 2020.
- [21] J. Pereira, R. Kobler, P. Ofner, A. Schwarz, and G. R. Müller-Putz, “Online detection of movement during natural and self-initiated reach-and-grasp actions from EEG signals,” *Journal of Neural Engineering*, vol. 18, no. 4, p. 046 095, 2021.
- [22] R. J. Kobler, E. Kolesnichenko, A. I. Sburlea, and G. R. Müller-Putz, “Distinct cortical networks for hand movement initiation and directional processing: An EEG study,” *NeuroImage*, vol. 220, p. 117 076, 2020.
- [23] M. R. Nuwer, “10-10 electrode system for EEG recording.,” *Clinical Neurophysiology: Official Journal of the International Federation of Clinical Neurophysiology*, vol. 129, no. 5, pp. 1103–1103, 2018.
- [24] C. Lopes-Dias, A. I. Sburlea, and G. R. Müller-Putz, “Online asynchronous decoding of error-related potentials during the continuous control of a robot,” *Scientific Reports*, vol. 9, no. 1, p. 17 596, 2019.
- [25] R. J. Kobler, A. I. Sburlea, C. Lopes-Dias, A. Schwarz, M. Hirata, and G. R. Müller-Putz, “Corneo-retinal-dipole and eyelid-related eye artifacts can be corrected offline and online in electroencephalographic and magnetoencephalographic signals,” *NeuroImage*, vol. 218, p. 117 000, 2020.

- [26] E. Larson, A. Gramfort, D. A. Engemann, *et al.*, *Mne-python*, version v1.3.1, Feb. 2023. DOI: 10.5281/zenodo.7671973. [Online]. Available: <https://doi.org/10.5281/zenodo.7671973>.
- [27] A. Gramfort, M. Luessi, E. Larson, *et al.*, “MEG and EEG data analysis with MNE-Python,” *Frontiers in Neuroscience*, vol. 7, no. 267, pp. 1–13, 2013. DOI: 10.3389/fnins.2013.00267.
- [28] X. Jiang, G.-B. Bian, and Z. Tian, “Removal of artifacts from EEG signals: a review,” *Sensors*, vol. 19, no. 5, p. 987, 2019.
- [29] D. J. McFarland, L. M. McCane, S. V. David, and J. R. Wolpaw, “Spatial filter selection for EEG-based communication,” *Electroencephalography and Clinical Neurophysiology*, vol. 103, no. 3, pp. 386–394, 1997.
- [30] A. C. Davison and D. V. Hinkley, *Bootstrap methods and their application*. Cambridge University Press, 1997.
- [31] T. E. Nichols and A. P. Holmes, “Nonparametric permutation tests for functional neuroimaging: A primer with examples,” *Human Brain Mapping*, vol. 15, no. 1, pp. 1–25, 2002.
- [32] E. Maris and R. Oostenveld, “Nonparametric statistical testing of EEG-and MEG-data,” *Journal of Neuroscience Methods*, vol. 164, no. 1, pp. 177–190, 2007.
- [33] C. M. Bishop and N. M. Nasrabadi, *Pattern Recognition and Machine Learning*. Springer, 2006, vol. 4.
- [34] B. Blankertz, S. Lemm, M. Treder, S. Haufe, and K.-R. Müller, “Single-trial analysis and classification of ERP components—A tutorial,” *NeuroImage*, vol. 56, no. 2, pp. 814–825, 2011.
- [35] O. Ledoit and M. Wolf, “Honey, I shrunk the sample covariance matrix,” *UPF Economics and Business Working Paper*, no. 691, 2003.
- [36] J. Xie and Z. Qiu, “The effect of imbalanced data sets on LDA: A theoretical and empirical analysis,” *Pattern Recognition*, vol. 40, no. 2, pp. 557–562, 2007.

- [37] J.-H. Xue and P. Hall, “Why does rebalancing class-unbalanced data improve AUC for linear discriminant analysis?” *IEEE Transactions on Pattern Analysis and Machine Intelligence*, vol. 37, no. 5, pp. 1109–1112, 2014.
- [38] G. Müller-Putz, R. Scherer, C. Brunner, R. Leeb, and G. Pfurtscheller, “Better than random? A closer look on BCI results,” *International Journal of Bioelectromagnetism*, vol. 10, no. 1, pp. 52–55, 2008.
- [39] E. Combrisson and K. Jerbi, “Exceeding chance level by chance: The caveat of theoretical chance levels in brain signal classification and statistical assessment of decoding accuracy,” *Journal of Neuroscience Methods*, vol. 250, pp. 126–136, 2015.
- [40] J.-B. Poline and M. Brett, “The general linear model and fMRI: Does love last forever?” *NeuroImage*, vol. 62, no. 2, pp. 871–880, 2012.
- [41] A. Schwarz, P. Ofner, J. Pereira, A. I. Sburlea, and G. R. Müller-Putz, “Decoding natural reach-and-grasp actions from human EEG,” *Journal of Neural Engineering*, vol. 15, no. 1, p. 016 005, 2017.
- [42] C. Guger, A. Schlogl, C. Neuper, D. Walterspacher, T. Strein, and G. Pfurtscheller, “Rapid prototyping of an EEG-based brain-computer interface (BCI),” *IEEE Transactions on Neural Systems and Rehabilitation Engineering*, vol. 9, no. 1, pp. 49–58, 2001.
- [43] H. S. Pulferer, B. Ásgeirsdóttir, V. Mondini, A. I. Sburlea, and G. R. Müller-Putz, “Continuous 2D trajectory decoding from attempted movement: across-session performance in able-bodied and feasibility in a spinal cord injured participant,” *Journal of Neural Engineering*, vol. 19, no. 3, p. 036 005, 2022.